# Dihydrogen Evolution by Protonation Reactions of Nickel(I)

**Thomas L. James, Lisheng Cai, Mark C. Muetterties, and R. H. Holm***

Department of Chemistry, Harvard University, Cambridge, Massachusetts 02138

*Received February 28, 1996*[⊗]

Nickel-mediated formation of $H_2$ by protonation of Ni(I) has been established and the kinetics of the process investigated. The diamagnetic complex $[Ni^{II}(psnet)](BF_4)_2$ was prepared and reduced to $[Ni^{I}(psnet)](BF_4)$ with $NaBH_4$ in THF (psnet = bis(5-(diphenylphosphino)-3-thiapentanyl)amine). Both complexes were structurally characterized by X-ray diffraction. $[Ni(psnet)]^{1+}$ was demonstrated to be an authentic Ni(I) complex with a $...(d_{z^2})^1$ ground state. Under appropriate conditions, $[Ni(psnet)]^+$ reacts with acids in nonaqueous media to give near-quantitative yields of $H_2$ according to the stoichiometry $Ni^I + H^+ \rightarrow Ni^{II} + {}^1/_2H_2$. Dihydrogen production was demonstrated to be directly related to Ni(I) oxidation. The reaction system $[Ni(psnet)]^+$/HCl/DMF, which gives $H_2$ yields of $\gtrsim$90%, was subjected to a kinetics analysis. The overall reaction $[Ni(psnet)]^+ + HCl \rightarrow [Ni(psnet)Cl]^+ + {}^1/_2H_2$ proceeds by two parallel pathways dependent on chloride concentration. Addition of $Bu_4NCl$ accelerates the reaction, whereas $(Bu_4N)(PF_6)$ decreases the rate. A two-term rate law is presented which includes contributions from both pathways, whose common initial step is protonation of Ni(I). Path A (low chloride concentration) involves the formation and collapse of nickel hydride chloride ion pairs; the rate-determining step is the minimal reaction $2Ni^{III}-H^- \rightarrow H_2 + 2Ni^{II}$. Path B (high chloride concentration) includes as the rate-limiting step collapse of a nickel hydride dichloride ion pair followed by the bimolecular reaction of two $Ni^{III}-H^-$ intermediates or reduction to $Ni^{II}-H^-$ by $Ni^I$ followed by protonation of the hydride. The relation of these results to the reactions of hydrogenase enzymes is considered.

## Introduction

Biomimetic research on [NiFe] hydrogenases[1,2] is now extensive[3−5] and has concentrated on structure modeling by synthesis of new complexes, often for comparison with Ni EXAFS of the enzymes and stabilization and EPR properties of Ni(III) and Ni(I) states. Our most recent contribution to this area is the demonstration that the physiological oxidation states of nickel, Ni(III,II,I), are unlikely to be traversed in any environment without accompanying alteration(s) in stereochemistry accountable in terms of the stereoelectronic preferences of the metal.[6] Functional modeling, on the other hand, is in a primitive stage of development. Nickel-mediated dihydrogen evolution, whether or not in the context of hydrogenase, has been brought about under four approaches: (i) reaction 1,

$$Ni^0 + H^+ \rightarrow Ni^{II}-H^- \xrightarrow{H^+} Ni^{II} + H_2 \qquad (1)$$

entailing protonation of Ni(0) complexes to form Ni(II) hydrides which are then protonated to yield Ni(II) and dihydrogen;[7] (ii) reactions 2, involving protonation of Ni(I) complexes to putative

$$Ni^I + H^+ \rightarrow Ni^{III}-H^- \xrightarrow{e^-} Ni^{II}-H^- \xrightarrow{H^+} Ni^{II} + H_2 \qquad (2a)$$

$$2Ni^{III}-H^- \rightarrow 2Ni^{II} + H_2 \qquad (2b)$$

nickel(III) hydrides which then react further to produce Ni(II) and dihydrogen[7b,8,9] by either (a) reduction and protonation events, the order of which is uncertain, or (b) bimolecular coupling of two nickel(III) hydrides; (iii) electrocatalysis in aqueous solution;[10−12] (iv) protonation of a binuclear nickel(II) phosphine−thiolate complex.[13] A number of the electrocatalytic studies were directed toward the reduction of carbon dioxide;[11] the potentials employed were far more negative than hydroge-

⊗ Abstract published in *Advance ACS Abstracts,* May 1, 1996.

(1) (a) Cammack, R.; Fernandez, V. M.; Schneider, K. In *The Bioinorganic Chemistry of Nickel*; Lancaster, J. R., Jr., Ed.; VCH Publishers, Inc.; New York, 1988; Chapter 8. (b) Moura, J. J. G.; Teixeira, M.; Moura, I.; LeGall, J. In *The Bioinorgnic Chemistry of Nickel*; Lancaster, J. R., Jr., Ed.; VCH Publishers, Inc.: New York, 1988; Chapter 9. (c) Cammack, R. *Adv. Inorg. Chem.* **1988**, *32*, 297. (d) Cammack, R. In *Bioinorganic Catalysis*; Reedijk, J., Ed.; Marcel Dekker, Inc.; New York, 1993; Chapter 7. (e) Kolodziej, A. F. *Prog. Inorg. Chem.* **1994**, *41*, 493.
(2) Albracht, S. P. J. *Biochim. Biophys. Acta* **1994**, *1188*, 167.
(3) Baidya, N.; Mascharak, P. K. *Trends Inorg. Chem.* **1993**, *3*, 275.
(4) Kovacs, J. A. *Adv. Inorg. Biochem.* **1994**, *9*, 173.
(5) Halcrow, M.; Christou, G. *Chem. Rev.* **1994**, *94*, 2421.
(6) James, T. L.; Smith, D. M.; Holm, R. H. *Inorg. Chem.* **1994**, *33*, 4869.
(7) (a) Tolman, C. A. *J. Am. Chem. Soc.* **1970**, *92*, 4217. (b) Sacconi, L.; Orlandini, A.; Midollini, S. *Inorg. Chem.* **1974**, *13*, 2850. (c) Rigo, P.; Bressan, M.; Basato, M. *Inorg. Chem.* **1979**, *18*, 860. (d) Cariati, F.; Ugo, R.; Bonati, F. *Inorg. Chem.* **1966**, *5*, 1128. (Formation of $H_2$ was implied but not documented.)
(8) Lahiri, G. K.; Schussel, L. J.; Stolzenberg, A. M. *Inorg. Chem.* **1992**, *31*, 4991.
(9) (a) Vlček, A., Jr.; Vlček, A. A. *Inorg. Chim. Acta* **1980**, *41*, 123. (b) Hsiao, Y.-M.; Chojnacki, S. S.; Hinton, P.; Reibenspies, J. H.; Darensbourg, M. Y. *Organometallics* **1993**, *12*. 870. (Dihydrogen formation from Ni(I) and acids was stated, but details were not reported.)
(10) Efros, L. L.; Thorp, H. H.; Brudvig, G. W.; Crabtree, R. H. *Inorg. Chem.* **1992**, *31*, 1722.
(11) (a) Fisher, B.; Eisenberg, R. *J. Am. Chem. Soc.* **1980**, *102*, 7361. (b) Bradley, M. G.; Tysak, T.; Graves, D. J.; Vlachopoulos, N. A. *J. Chem. Soc., Chem. Commun.* **1983**, 349. (c) Beley, M.; Collin, J.-P.; Ruppert, R. P.; Sauvage, J.-P. *J. Am. Chem. Soc.* **1986**, *108*, 7461. (d) Grant, J. L.; Goswani, K.; Spreer, L. O.; Otvos, J. W.; Calvin, M. *J. Chem. Soc., Dalton Trans.* **1987**, 2105. (e) Collin, J.-P.; Jouaiti, A.; Sauvage, J.-P. *Inorg. Chem.* **1988**, *27*, 1986. (f) Shinoya, M.; Kimura, E.; Iitaka, Y. *J. Am. Chem. Soc.* **1990**, *112*, 9237.
(12) (a) Căluşaru, A.; Voicu, V. *Electroanal. Chem. Interfacial Electrochem.* **1973**, *43*, 257. (b) Căluşaru, A.; Bănică, F. G. *Electroanal. Chem. Interfacial Electrochem.* **1973**, *47*, 190. (c) Bănică, F. G.; Căluşaru, A. *J. Electroanal. Chem.* **1983**, *145*, 389. (d) Bănică, F. G. *J. Electroanal. Chem.* **1984**, *171*, 351; *Talanta* **1985**, *32*, 1145. (e) Bănică, F. G.; Diacu, E.; Luca, G. *Bull. Soc. Chim. Belg.* **1987**, *96*, 485. (f) Bănică, F. G.; Florea, M.; Moraru, M. *J. Electroanal. Chem.* **1990**, *285*, 281. (g) Bănică, F. G.; Diacu, E. *Collect. Czech. Chem. Commun.* **1991**, *56*, 140. (h) Bănică, F. G. *Bull. Soc. Chim. Fr.* **1991**, *128*, 697.
(13) Franolic, J. D.; Millar, M. M. *Abstracts*, 205th National Meeting of the American Chemical Society, Denver, CO, 1993; INOR 534; American Chemical Society: Washington, DC, 1993.

S0020-1669(96)00216-9 CCC: $12.00 

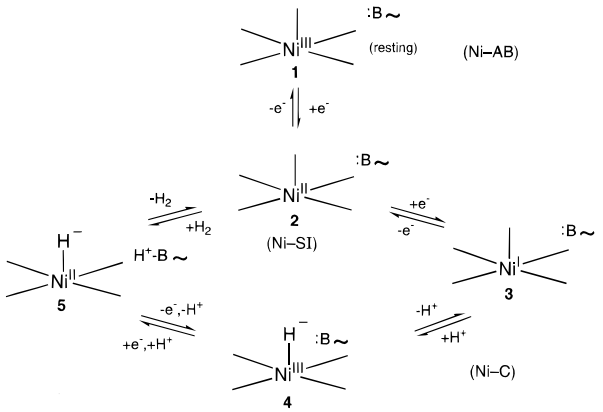


**Figure 1.** Minimal scheme for the nickel-mediated reaction $2H^+ + 2e^- \rightleftarrows H_2$. B is a neighboring base; if the scheme were to be related to hydrogenase, the Ni−C designation would best apply to **3** or **4** with $S = {}^1/_2$. A number of related reaction cycles have been proposed.[1]

nase potentials or the $H^+/H_2$ potential at pH 7 (−655 mV vs SCE), and dihydrogen was formed as a byproduct. These reductive conditions may subsume approaches i and ii, but in no case was the reactive nickel species identified.[11,12] With several recent exceptions,[10,12h] approach iii was not pursued in relation to hydrogenase.

Our present investigation centers on nickel-mediated dihydrogen evolution, for which a working hypothesis is represented by the scheme in Figure 1. The catalytic cycle contains reaction 2a and thus approach ii-a to dihydrogen evolution. There has been considerable recent progress in the generation, EPR properties, and redox chemistry of various Ni(I) complexes;[3−5,14−16] however, very few of these complexes have been isolated in substance[16] nor has their reactivity toward protic acids been tested. Initial complexes in reactions 2 were generated in situ; in addition, assertions about dihydrogen formation in reactions 2 are still speculative. We have sought routes to Ni(I) species reactive toward Brönsted acids but sufficiently stable to be isolated. The approach taken in this work exploits the redox versatility of nickel complexes formed with conformationally flexible ligands containing mixed hard−soft donor sets.[6] Here we have utilized fully characterized Ni(II,I) complexes of the pentadentate ligand bis(5-diphenylphosphino)-3-thiapentanyl)amine and show that the Ni(I) species is capable of stoichiometric dihydrogen evolution. Inasmuch as the $H_2$-evolving system developed here includes neither a Ni−Fe complex nor thiolate ligation at the nickel site, properties of the active site of *Desulfovibrio gigas* (*D. gigas*) hydrogenase established by crystallography,[17] it cannot be construed, and is not intended, as a close functional analogue of hydrogenase. It is, instead, a first-generation experimental representation of nickel-mediated dihydrogen evolution whose reactivity and mechanism indicate certain features obligatory to a functional analogue.

## Experimental Section

**Preparation of Compounds.** Unless otherwise noted, all operations were carried out under a pure dinitrogen atmosphere. Reagents were commercial samples and were not purified further. The compounds 2-(diphenylphosphino)ethanethiol[18] (psh), and $[Ni(NS_3{}^{tBu})H](BPh_4)$[19] ($NS_3{}^{tBu}$ = tris[(*tert*-butylthio)ethyl]amine) were prepared by literature methods. Solvents were dried by standard methods and thoroughly degassed prior to use.

**Bis(5-(diphenylphosphino)-3-thiapentanyl)amine (psnet).** A solution of Na(psh), prepared from 0.55 g (23.9 mmol) of sodium and 5.88 g (23.9 mmol) of psh in 100 mL of ethanol, was added dropwise to a solution of 2.13 g (11.9 mmol) of bis(2-chloroethyl)amine (generated from the hydrochloride with NaOEt) in 100 mL of ethanol at 0 °C. The reaction mixture was allowed to warm to room temperature with stirring and was stirred for an additional 12 h, during which time a white precipitate formed. The mixture was filtered, and the filtrate was concentrated in vacuo. The resulting white paste was dissolved in toluene to remove residual NaCl, the mixture was filtered, and the filtrate was taken to dryness in vacuo. The product was obtained as 5.5 g (82%) of a sticky white solid; analytical data indicate an ethanol monosolvate. FAB-MS (3-nitrobenzyl alcohol): *m/z* 562 (M + H⁺ − EtOH). $^1$H NMR ($C_6D_6$): $\delta$ 2.25−2.28 (m, 4), 2.34 (t, 4), 2.44 (t, 4), 2.52−2.55 (m, 4), 5.02 (s, 1), 7.00−7.05 (m, 12), 7.34−7.38 (m, 8). Anal. Calcd for $C_{34}H_{43}ONP_2S_2$: C, 67.19; H, 7.13; N, 2.30. Found: C, 67.30; H, 6.85; N, 2.34.

**[Bis(5-(diphenylphosphino)-3-dithiapentanyl)amine]nickel(II) Tetrafluoroborate ([Ni(psnet)](BF$_4$)$_2$).** A solution of 3.33 g (9.80 mmol) of $[Ni(OH_2)_6](BF_4)_2$ in 100 mL of ethanol was added dropwise to a solution of 5.50 g (9.80 mmol) of psnet in 100 mL of ethanol. A deep purple precipitate formed immediately. The reaction mixture was stirred for 2 h, and the solid was collected by filtration. This material was washed thoroughly with ether, toluene, tetrahydrofuran (THF), and again with ether; it was recrystallized from methanol/ether. The product was obtained as 4.7 g (61%) of a purple microcrystalline solid. FAB-MS (3-nitrobenzyl alcohol): *m/z* 706 (M − $BF_4^-$). Visible spectrum (propylene carbonate): $\lambda_{max}$ ($\epsilon_M$, $M^{-1}$ $cm^{-1}$) 526 (1490), 607 (sh, 1160) nm. $^1$H NMR (acetone): $\delta$ 1.45 (t, 4), 3.05 (t, 4), 3.31 (br, 4), 3.44 (t, 4), 7.46 (m, 8), 7.66 (m, 12). Anal. Calcd for $C_{32}H_{37}B_2F_8NNiP_2S_2$: C, 48.40; H, 4.70; N, 1.76; Ni, 7.39. Found: C, 48.58; H, 5.06; N, 1.64; Ni, 7.28. The compound was additionally identified by an X-ray structure determination.

**[Bis(5-(diphenylphosphino)-3-thiapentanyl)amine]nickel(I) Tetrafluoroborate ([Ni(psnet)](BF$_4$)).** To a solid mixture of 1.72 g (2.20 mmol) of $[Ni(psnet)](BF_4)_2$ and 0.099 g (2.60 mmol) of $NaBH_4$ was added 100 mL of THF with rapid stirring. A purple slurry formed initially; over 1 h the reaction mixture became a deep brown-green solution, from which a light green powder precipitated over the next 5 h. The precipitate was allowed to settle overnight and was collected by filtration. To remove excess $NaBF_4$, the green solid was dissolved in acetonitrile, the mixture was filtered, and the solvent was removed in vacuo. The crude product was washed extensively with ether and recrystallized from THF/ether to afford the pure product as 0.92 g (60%) of a green microcrystalline solid. Absorption spectrum (DMF): $\lambda_{max}$ ($\epsilon_M$, $M^{-1}$ $cm^{-1}$) 259 (13 200), 357 (5500), 949 (107) nm. Anal. Calcd. for $C_{32}H_{37}BF_4NNiP_2S_2$: C, 54.35; H, 5.27; N, 1.98; Ni, 8.30. Found: C, 54.20; H, 5.15; N, 1.88; Ni, 8.19. The compound was additionally identified by an X-ray structure determination.

**Chloro[bis(5-(diphenylphosphino)-3-thiapentanyl)amine]nickel(II) Chloride ([Ni(psnet)Cl]Cl).** A solution of 0.86 g (2.6 mmol) of $[Ni(OH_2)_6]Cl_2$ in 100 mL of ethanol was added dropwise to a solution of 2.0 g (3.6 mmol) of psnet in 100 mL of ethanol. The resultant deep purple solution was stirred for 2 h; the solvent was removed in vacuo, yielding a purple glass which was washed thoroughly with ether. The solid was dissolved in *ca*. 75 mL of dimethylformamide (DMF), forming a pastel green solution. Slow addition of ether followed by filtration afforded the product as 1.85 g (75%) of light green powder. FAB-MS (DMF): *m/z* (M − Cl) 654. Absorption spectrum (DMF): $\lambda_{max}$ ($\epsilon_M$, $M^{-1}$ $cm^{-1}$) 259 (14 600), 630 (21), 968 (sh, 24), 1050 (27) nm. Anal. Calcd for $C_{32}H_{37}Cl_2NNiP_2S_2$: C, 55.60; H, 5.39; N, 2.03. Found: C, 55.50; H, 5.29; N, 2.00.

(14) (a) Baidya, N.; Olmstead, M.; Mascharak, P. K. *Inorg. Chem.* **1991**, *30*, 929. (b) Baidya, N.; Olmstead, M.; Mascharak, P. K. *J. Am. Chem. Soc.* **1992**, *114*, 9666. (c) Baidya, N.; Noll, B. C.; Olmstead, M. M.; Mascharak, P. K. *Inorg. Chem.* **1992**, *31*, 2999. (d) Baidya, N.; Olmstead, M. M.; Whitehead, J. P.; Bagyinka, C.; Maroney, M. J.; Mascharak, P. K. *Inorg. Chem.* **1992**, *31*, 3612.
(15) Farmer, P. J.; Reibenspies, J. H.; Lindahl, P. A.; Darensbourg, M. Y. *J. Am. Chem. Soc.* **1993**, *115*, 4665.
(16) Suh, M. P.; Kim, H. K.; Kim, M. J.; Oh, K. Y. *Inorg. Chem.* **1992**, *31*, 3620.
(17) Volbeda, A.; Charon, M.-H.; Piras, C.; Hatchikian, E. C.; Frey, M.; Fontecilla-Camps, J. C. *Nature* **1995**, *373*, 580.
(18) Chatt, J.; Dilworth, J. R.; Schmutz, J. A.; Zubieta, J. A. *J. Chem. Soc., Dalton Trans.* **1979**, 1595.
(19) Stavropoulos, P.; Muetterties, M. C.; Carrié, M.; Holm, R. H. *J. Am. Chem. Soc.* **1991**, *113*, 8485.

**Bis[1,2-bis(diphenylphosphino)ethane]hydridonickel(II) Tetrafluoroborate ([Ni(diphos)$_2$H](BF$_4$).** The following procedure is somewhat simpler and affords a higher yield than that originally reported.[20] To a stirred solution of 0.95 g (1.1 mmol) of [Ni(diphos)$_2$][21] in 40 mL of THF was added dropwise 220 $\mu$L (1.2 mmol) of HBF$_4$·Et$_2$O (85%, Aldrich). The resulting deep orange solution was stirred for 30 min, during which a microcrystalline orange solid separated from the solution. The solid was isolated by filtration, washed with ether, and recrystallized from acetone/ether. The product was obtained as 0.75 g (72%) of an orange crystalline solid. $^1$H NMR ($CD_2Cl_2$): $\delta$ −13.03 (quintet, 1), 2.38 (s, 8), 7.14 (br, 16), 7.19 (t, 16), 7.37 (t, 8).

**Reactions of [Ni(psnet)](BF$_4$) with Acids.** All reactions were carried out in 20 mL sealed vials using butyl rubber caps. Solutions containing 15−20 mg (*ca*. 5 mM) of [Ni(psnet)](BF$_4$) in 5 mL of propylene carbonate (PC) or DMF were transferred to the vials and sealed under dinitrogen. Acids were added using a gastight syringe; reaction mixtures were rapidly stirred. Dihydrogen production was monitored with a Varian Model 3700 gas chromatograph equipped with a thermal conductivity detector, strip chart recorder, and integrator. Resolution of headspace gases was accomplished with a 2-m column of 0.6-cm-i.d. aluminum tubing packed with 60/80 mesh 5-Å molecular sieves, operating at ambient temperature. Argon was used as the carrier gas. Samples of headspace gas (200 $\mu$L) were removed from the sealed vials with a Pressure-Lok syringe and injected directly into the gas chromatograph. Dihydrogen yields were calculated by comparison of integrated peak areas with standards prepared under identical conditions. In experiments that determined the time course of dihydrogen evolution, aliquots were removed from the reaction solutions at 30−45 s for the first *ca*. 4 min of the reaction and at 2−9 min intervals thereafter. The decrease in headspace pressure caused by the removal of multiple aliquots was considered in the calculation of dihydrogen yields.

**Kinetics Measurements.** The kinetics of dihydrogen formation in the reaction of [Ni(psnet)]$^+$ with HCl in DMF were investigated. All reactions were performed under strictly anaerobic conditions. Solvent DMF (Aldrich, 99+%, 1.1 mM water as determined by Karl Fischer titration) was stored over 3−4-Å molecular sieves in an inert atmosphere box prior to use. The acid source was 1.0 M HCl in diethyl ether (Aldrich, anhydrous) added as aliquots to DMF solutions; the titer of the ether solution was monitored periodically. Before use, (Bu$_4$N)(PF$_6$) (Aldrich, 98%) was recrystallized from absolute ethanol and dried in vacuo for 48 h, and Bu$_4$NCl (Fluka, 99%) was dried in vacuo for 24 h.

Reactions were monitored with a Varian Cary 3 spectrophotometer equipped with a cell compartment thermostated at 25.0 ± 0.5 °C. Dihydrogen evolution was followed by monitoring the decay of [Ni(psnet)]$^+$ absorbance at 380 nm, where overlap with product absorbances is minimized. The tight isosbestic point at 272 nm indicates no measurable accumulation of intermediates. Initial concentrations in the reaction systems were [[Ni(psnet)]$^+$] = 0.420−2.70 mM and [HCl] = 5.01−48.9 mM, depending on the reaction rate. In reactions designed to determine the effects of Bu$_4$NCl and (Bu$_4$N)(PF$_6$) on reaction rate, aliquots of stock solutions of these compounds in DMF were added to a solution of [Ni(psnet)]$^+$ prior to the addition of HCl. Initial concentrations were [Bu$_4$NCl] = 0.00120−0.600 M and [(Bu$_4$N)(PF$_6$)] = 0.0125−0.508 M. Computations in data analysis were performed with the commercial programs *Kaleidagraph* and *Igor*.

**Collection and Reduction of X-ray Data.** Diffraction-quality crystals of [Ni(psnet)](BF$_4$)$_2$ (purple prisms) and [Ni(psnet)](BF$_4$) (green elongated plates) were obtained by diffusion of ether into solutions of the compounds in methanol and THF, respectively. Crystals were mounted in Paratone-N oil and attached to glass fibers. Diffraction data were collected using graphite-monochromatized Mo K$\alpha$ radiation on a Siemens R3m/v four-circle automated diffractometer equipped with a Siemens LT-2 cryostat operating at 233 K. Unit cell parameters were obtained by least-squares refinement of machine-centered reflections. Intensities of three standard reflections monitored every 97 reflections indicated no significant decay during the data collections. Crystallographic data are summarized in Table 1. Corrections for Lorentz and polarization effects were applied using the program XDISK of the SHELXTL PLUS program package; empirical absorption corrections were made with XEMP. Assignments of space groups from statistics and systematic absences were confirmed by successful solutions and refinements of the structures.

**Table 1.** Summary of Crystallographic Data[a]

| | [Ni(psnet)](BF$_4$)$_2$ | [Ni(psnet)](BF$_4$) |
|---|---|---|
| formula | $C_{32}H_{37}B_2F_8N_1Ni_1P_2S_2$ | $C_{32}H_{37}B_1F_4N_1Ni_1P_2S_2$ |
| fw | 794.0 | 707.2 |
| cryst syst | monoclinic | triclinic |
| space group | $P2_1/c$ | $P\bar{1}$ |
| $Z$ | 4 | 2 |
| $a$, Å | 10.887 (3) | 10.701 (3) |
| $b$, Å | 14.331 (3) | 12.978 (3) |
| $c$, Å | 23.057 (5) | 13.138 (3) |
| $\alpha$, deg | | 109.97 (2) |
| $\beta$, deg | 103.43 (2) | 96.53 (2) |
| $\gamma$, deg | | 102.77 (2) |
| $V$, Å$^3$ | 3499.0 (14) | 1636.3 (8) |
| $\rho_{calc}$, g/cm$^3$ | 1.51 | 1.44 |
| $\mu$, mm$^{-1}$ | 0.83 | 0.87 |
| $R$,[b] $R_w$,[c] % | 6.12, 6.48 | 4.38, 4.26 |

[a] Obtained at $T$ = 233 K with graphite-monochromatized Mo K$\alpha$ radiation ($\lambda$ = 0.710 69 Å). [b] $R = \sum||F_o| - |F_d||/\sum|F_o|$. [c] $R_w = \{\sum[w(|F_o| - |F_c|^2)]/\sum[w|F_o|^2]\}^{1/2}$.

**Solution and Refinement of Structures.** Initial structure solutions were obtained either by direct methods or Patterson maps. All non-hydrogen atoms not located in these solutions were found by successive Fourier or difference Fourier maps with intervening cycles of least-squares refinement. All non-hydrogen atoms were described anisotropically in both structures. In the final stages of the refinements, hydrogen atoms were placed 0.96 Å from bonded carbon atoms and 0.90 Å from bonded nitrogen atoms and were assigned a temperature factor of 0.08 Å$^2$. Final difference Fourier maps generally exhibited residual electron density only near anions, indicating possible disorder that was not refined further. Final $R$-values are set out in Table 1.[22]

**Other Physical Measurements.** Absorption spectra were recorded on Varian 2390 and Perkin-Elmer Lambda 4C spectrophotometers. NMR spectra were obtained on a Bruker AM-400 spectrometer. EPR spectra were determined at 120 K on a Bruker ESP 300-E spectrometer operating at X-band frequencies. Spin concentrations were determined from a calibration curve derived from the integrated spectra of standard solutions of CuSO$_4$ in glycerol:water(1:1 (v/v)). Integrated Ni(I) spectra were corrected for transition probability differences[23] between sample and standard. Electrochemical measurements were performed under a dinitrogen atmosphere with use of an EG&G Model 263 potentiostat. For cyclic voltammetry experiments, 1−2 mM solutions containing 0.1 M Bu$_4$NPF$_6$ supporting electrolyte and a Pt disc working electrode were used. Potentials were determined vs a SCE reference electrode. Conductance measurements were performed with a Fisher Scientific digital conductivity meter equipped with a Pt probe.

## Results and Discussion

**Nickel(II,I) Complexes. (a) Synthesis and Properties.** The objective of this investigation required a Ni(I) complex sufficiently stable to permit full structural and electronic characterization and reactive toward protic sources. The procedure employed utilizes pentadentate ligand psnet and is outlined in Figure 2. Upon recrystallization from methanol/ether, [Ni(psnet)](BF$_4$)$_2$ was obtained as deep purple prisms that are soluble in acetonitrile, acetone, propylene carbonate, and DMF. The compound is air-stable for days in solution and indefinitely stable in the solid state. The complex [Ni(psnet)]$^{2+}$ is diamagnetic in acetone ($^1$H NMR) and exhibits an absorption spectrum in PC, shown in Figure 3, that resembles that of low-spin Ni(II) species in distorted trigonal bipyramidal environments.[24]

(20) Schunn, R. A. *Inorg. Chem*. **1970**, *9*, 394.
(21) Chatt, J.; Hart, F. A.; Watson, H. R. *J. Chem. Soc*. **1962**, 2537.
(22) See paragraph at the end of this article concerning Supporting Information.
(23) Aasa, R.; Vänngård, T. *J. Magn. Reson*. **1975**, *19*, 308.

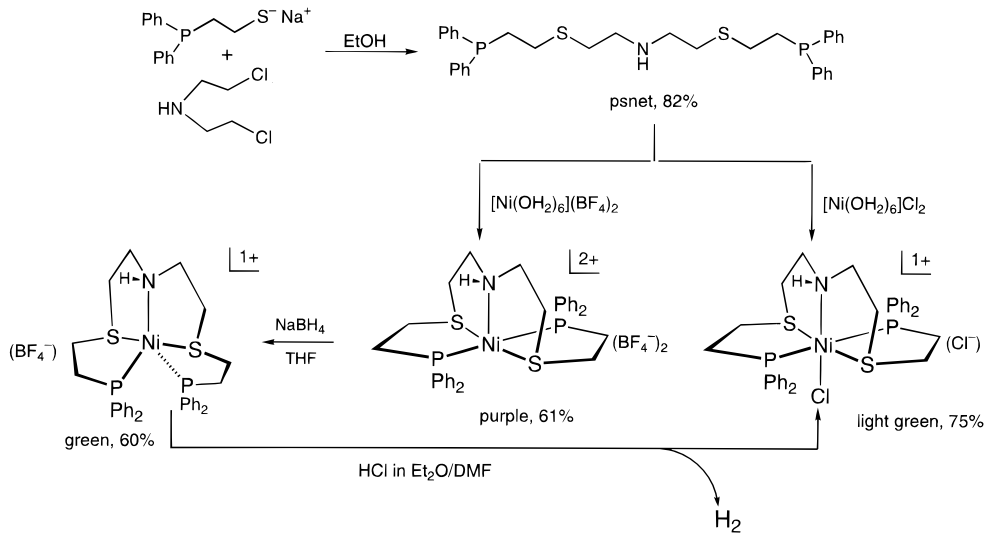


**Figure 2.** Preparation of Ni(II,I) complexes utilized in this work. The structures of $[Ni(psnet)]^{2+,1+}$ have been established by X-ray determinations; the structure of $[Ni(psnet)Cl]^{1+}$ is proposed.

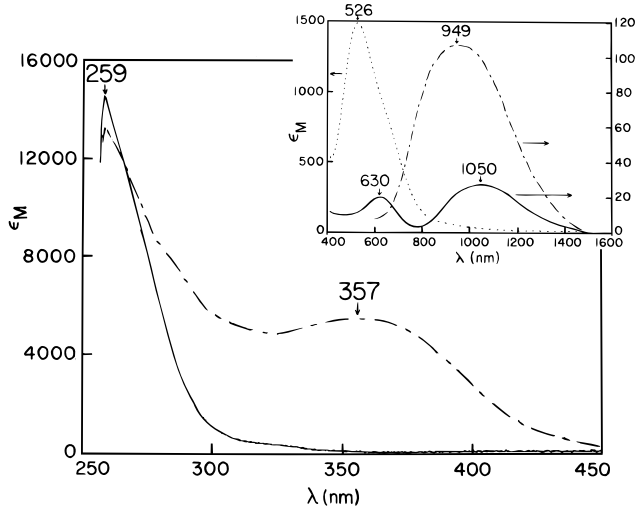


**Figure 3.** Absorption spectra of Ni(II,I) complexes: (···) $[Ni(psnet)](BF_4)_2$ in propylene carbonate; (– - –) $[Ni(psnet)](BF_4)$ in DMF; (—) [Ni(psnet)Cl]Cl in DMF. Band maxima are indicated.

The spectrum in PC solution reveals a characteristically intense $^1A_1' \rightarrow {}^1E'$ transition at 526 nm; the low-intensity $^1A_1' \rightarrow {}^1E''$ feature expected at higher energies is obscured by charge-transfer transitions. A shoulder near 600 nm presumably reflects the lowering of symmetry from idealized $D_{3h}$ coordination.

Reduction of $[Ni(psnet)]^{2+}$ with $NaBH_4$ in THF affords green $[Ni(psnet)]^+$, obtained in 60% yield as the $BF_4^-$ salt. The compound is soluble in acetonitrile, acetone, PC, THF, and DMF; in solution it is oxidized within minutes to $[Ni(psnet)]^{2+}$ but is stable to air for hours in the solid state. The solid state magnetic moment of 2.10$\mu_B$ (room temperature) indicates an $S = {}^1/_2$ ground state. A single broad band at 949 nm in the absorption spectrum in DMF solution (Figure 3) is reminiscent of the unresolved d−d spectra of certain trigonal bipyramidal Cu(II) complexes.[24a,25] Because d−d spectral/structure correlations of Ni(I) complexes are incompletely developed, an assignment of stereochemistry based on the absorption spectrum is not reliable. Structural and other electronic properties of $[Ni(psnet)]^+$ are described below.

The complex $[Ni(psnet)Cl]^+$ was required to identify the nickel-containing product of the protonation reaction of $[Ni(psnet)]^+$ with HCl. It was obtained as the light green chloride salt which in ethanol solution exists as purple low-spin $[Ni(psnet)]^{2+}$ according to the absorption spectrum. However, a DMF solution has the light green color of the solid, and chloride binding was demonstrated by FAB-MS and the absorption spectrum (Figure 3). The latter is typical of octahedral Ni(II),[24] exhibiting a split band of parentage $^3A_{2g} \rightarrow {}^3T_{2g}$ at 968 and 1050 nm and the $^3A_{2g} \rightarrow {}^3T_{1g}$ transition at 630 nm. The third octahedral feature at higher energies was obscured by charge-transfer absorption. The solid state magnetic moment of 3.12 $\mu_B$ (room temperature) is also consistent with an octahedral structure.

**(b) Structures.** The crystallographically determined structures of five-coordinate $[Ni(psnet)]^{2+,1+}$ are presented in Figure 4; selected metric parameters are set out in Table 2. These are the first structures of nickel complexes with $NP_2S_2$ coordination spheres. Both approach idealized $C_2$ microsymmetry, with the pseudosymmetry axis coincident with the Ni−N bond axis. The structure of $[Ni(psnet)]^{2+}$ is distorted from either the square pyramidal (SP) or trigonal bipyramidal (TBP) limit. The bond angles P(1)−Ni−N(1) = 103.4(3)° and P(2)−Ni−N(1) = 112.3(3)° are between the limits for the two structures, as is P(1)−Ni−P(2) = 144.3(1)°. The angle S(1)−Ni−S(2) = 176.1(1)° is consistent with either geometry; in the TBP limit the sulfur atoms are in axial positions. The Ni−N and mean Ni−P and Ni−S bond distances are comparable to those in other low-spin Ni(II) complexes with related donor sets.[26]

Upon reduction of $[Ni(psnet)]^{2+}$ to $[Ni(psnet)]^+$, the P(1)−Ni−N and P(2)−Ni−N angles expand to 115.6(1) and 119.8(1)°, respectively, while the P(1)−Ni−P(2) angle contracts to 124.6(1)°. Although the S(1)−Ni−S(2) angle decreases by *ca*. 10° (to 166.5(1)°), the overall angular changes are in the direction of TBP coordination, in which sulfur atoms are axially positioned. Because of the small number of structurally

(24) (a) Lever, A. B. P. *Inorganic Electronic Spectroscopy*; Elsevier: New York, 1984, Chapter 6. (b) Sacconi, L.; Mani, F.; Bencini, A. In *Comprehensive Coordination Chemistry*; Wilkinson, G., Ed.; Pergamon Press: Oxford, U.K., 1987; Vol. 5, pp 1−347.
(25) Tyagi, S.; Hathaway, B.; Kremer, S.; Stratemeier, H.; Reinen, D. *J. Chem. Soc., Dalton Trans.* **1984**, 2087.
(26) (a) Haugen, L. P.; Eisenberg, R. *Inorg. Chem.* **1969**, *8*, 1072. (b) Dapporto, P.; Sacconi, L. *J. Chem. Soc. A* **1970**, 1804. (c) Bianchi, A.; Dapporto, P.; Fallani, G.; Ghilardi, C. A.; Sacconi, L. *J. Chem. Soc., Dalton Trans.* **1973**, 641. (d) DiVaira, M.; Sacconi, L. *J. Chem. Soc., Dalton Trans.* **1975**, 493. (e) Orpen, A. G.; Brammer, F. H.; Allen, O. K.; Watson, R. T. *J. Chem. Soc., Dalton Trans.* **1989**, *Suppl. S1*.

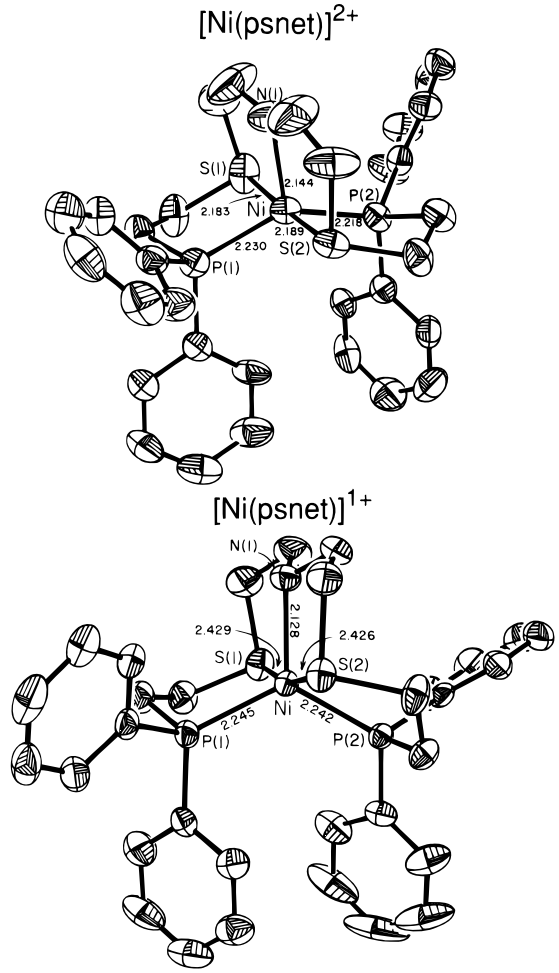


**Figure 4.** Structures of $[Ni(psnet)]^{2+}$ (top) and $[Ni(psnet)]^{+}$ (bottom) showing 40% and 50% probability ellipsoids, respectively, the atom labeling scheme, and selected bond distances which illustrate the lengthening of the Ni−S bonds upon reduction.

**Table 2.** Selected Interatomic Distances (Å) and Angles (deg) in $[Ni(psnet)](BF_4)_2$ (**I**) and $[Ni(psnet)](BF_4)$ (**II**)

| **I** | | **II** | |
|---|---|---|---|
| Ni(1)−S(1) | 2.183(3) | Ni(1)−S(1) | 2.429(1) |
| Ni(1)−S(2) | 2.189(3) | Ni(1)−S(2) | 2.426(1) |
| Ni(1)−P(1) | 2.230(3) | Ni(1)−P(1) | 2.245(2) |
| Ni(1)−P(2) | 2.218(3) | Ni(1)−P(2) | 2.242(2) |
| Ni(1)−N(1) | 2.144(9) | Ni(1)−N(1) | 2.128(4) |
| S(1)−Ni(1)−S(2) | 176.1(1) | S(1)−Ni(1)−S(2) | 166.5(1) |
| S(1)−Ni(1)−P(1) | 89.3(1) | S(1)−Ni(1)−P(1) | 87.2(1) |
| S(2)−Ni(1)−P(1) | 92.1(1) | S(2)−Ni(1)−P(1) | 100.3(1) |
| S(1)−Ni(1)−P(2) | 92.3(1) | S(1)−Ni(1)−P(2) | 97.6(1) |
| S(2)−Ni(1)−P(2) | 88.8(1) | S(2)−Ni(1)−P(2) | 87.4(1) |
| P(1)−Ni(1)−P(2) | 144.3(1) | P(1)−Ni(1)−P(2) | 124.6(1) |
| S(1)−Ni(1)−N(1) | 88.3(3) | S(1)−Ni(1)−N(1) | 83.6(1) |
| S(2)−Ni(1)−N(1) | 87.8(3) | S(2)−Ni(1)−N(1) | 83.1(1) |
| P(1)−Ni(1)−N(1) | 103.4(3) | P(1)−Ni(1)−N(1) | 115.6(1) |
| P(2)−Ni(1)−N(1) | 112.3(3) | P(2)−Ni(1)−N(1) | 119.8(1) |

characterized TBP Ni(I) complexes with similar ligands, dimensional comparisons are limited. We note that the mean Ni−P distance in $[Ni(psnet)]^{+}$ (2.244 Å) is close to the mean Ni−P equatorial distance in $[Ni\{P(CH_2CH_2PPh_2)_3\}]^{+}$ (2.219 Å)[27] and $[Ni\{P(CH_2CH_2PPh_2)_3\}I]$ (2.268 Å).[28] Also, the mean Ni−S axial distance of 2.428 Å is 0.07 Å longer than the mean Ni−S equatorial distance in the only other structurally defined TBP Ni(I) complex with thioether ligation.[19] However, the most important structural result is the *lengthening* of Ni−S bond lengths by 0.24−0.25 Å, while the Ni−N and Ni−P distances are nearly constant, their changes being ≲0.03 Å. This requires that the added electron occupy an antibonding MO concentrated along the S−Ni−S axial portion of the coordination unit (vide infra).

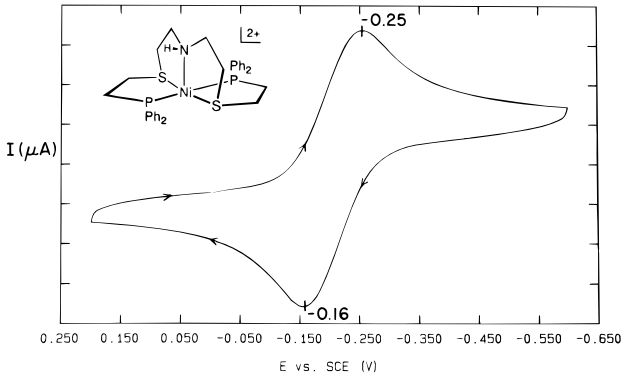


**Figure 5.** Cyclic voltammogram (50 mV/s) of $[Ni(psnet)]^{2+}$ in propylene carbonate solution. Peak potentials are indicated ($E_{1/2}$ = −0.21 V vs SCE).

**(c) Electron Transfer.** The cyclic voltammogram of $[Ni(psnet)]^{2+}$ in PC, shown in Figure 5, reveals a one-electron reduction at $E_{1/2} = -0.21$ V that is electrochemically quasi-reversible and chemically reversible. The peak current function $i_p/\nu^{1/2}$ is independent of scan rate, and $i_{pa}/i_{pc} \approx 1$ at scan rates of 20−200 mV/s. Similar behavior was observed in acetonitrile and DMF solutions using both glassy carbon and Pt disc electrodes. Coulometric reduction at a Pt gauze electrode at −0.37 V ($E_{1/2} = -0.17$ V) induces the passage of 0.96 F, while subsequent oxidation at 0.03 V results in the transfer of 0.95 F, indicating essentially no decomposition over the 1-h time scale of the experiment. Indeed, the electrolytic cycle may be repeated four times in sequence without appreciable deterioration of the electroactive species. The cyclic voltammogram of $[Ni(psnet)]^{+}$ is identical to that in Figure 5.

A second quasi-reversible one-electron reduction (not shown) of $[Ni(psnet)]^{2+}$, attributed to a Ni(I)/Ni(0) couple, is observed at $E_{1/2} = -1.36$ V in PC solution. A notable feature of this couple is the large peak-to-peak separation of 340 mV at the moderate scan rate of 50 mV/s, a property consistent with a rate-limiting structural change[29] upon reduction to Ni(0). Given the tendency of Ni(0) to form tetrahedral complexes with soft donor sets, the most reasonable structural change associated with this couple is decoordination of the secondary amine, affording a four-coordinate complex with $P_2S_2$ ligation. We have recently demonstrated the decoordination of two pyridyl ligands from a six-coordinate Ni(II) complex upon reduction to Ni(I), leaving a $P_2S_2$ coordination sphere.[6] Oxidation of $[Ni(psnet)]^{2+}$ in PC and acetonitrile is irreversible, with $E_{pa} \gtrsim 1.0$ V.

**(d) Ground State of $[Ni(psnet)]^{1+}$.** The EPR spectrum of $[Ni(psnet)]^{1+}$ in frozen 2-MeTHF/acetonitrile solution, presented in Figure 6, is rhombic with $g_1 = 2.21$, $g_2 = 2.13$, and $g_3 = 2.01$. Each line is split into a triplet by coupling with two equivalent $^{31}P$ nuclei ($a_1 = 45$ G, $a_2 = 40$ G, $a_3 = 44$ G); no $^{14}N$ hyperfine splitting was observed. Spin quantitation gave 0.97 spin/Ni. The spectrum of $[Ni(psnet)]^{+}$ in fluid THF solution at ambient temperature is a triplet with $g_{av} = 2.12$ and $a_{av} = 42$ G.

The EPR spectra demonstrate metal-centered reduction, and the observation that $g_1$, $g_2 > g_3 \approx 2$ is consonant with Ni(I)

(27) Cecconi, F.; Midollini, S.; Orlandini, A. *J. Chem. Soc., Dalton Trans.* **1983**, 2263.
(28) Dapporto, P.; Sacconi, L. *Inorg. Chim. Acta* **1980**, *39*, 61.
(29) Geiger, W. E. *Prog. Inorg. Chem.* **1985**, *33*, 275.

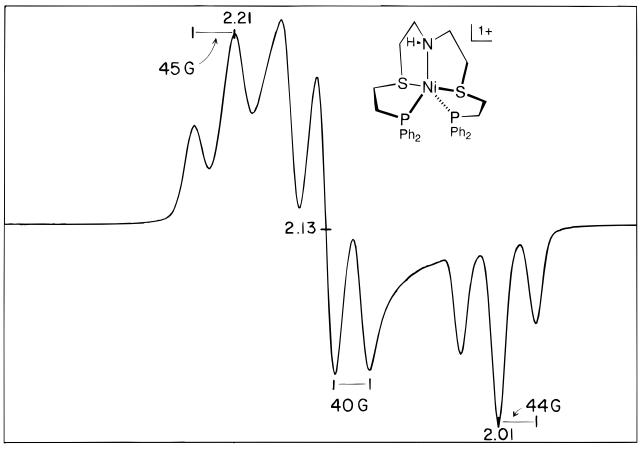


**Figure 6.** EPR spectrum of $[Ni(psnet)]^+$ in 7/3 2-MeTHF:MeCN (v/v) at 120 K; g-values and $a(^{31}P)$ values are indicated.

with the odd electron in the $d_{z^2}$ orbital.[30] This in turn is consistent with the *ca.* 0.24-Å expansion of the Ni−S bonds upon reduction to $[Ni(psnet)]^+$. This observation has several precedents. For example, the axial Ni−N and Ni−I bonds in $[Ni\{N(CH_2CH_2PPh_2)_3\}I]$[28] are longer by 0.13 and 0.30 Å, respectively, compared to the corresponding bond lengths in $[Ni\{N(CH_2CH_2PPh_2)_3\}I]^+$.[26b] A similar change in axial Ni−N bond lengths was found in $[Ni\{N(CH_2CH_2AsPh_2)_3\}I]$,[28] as compared with the Ni(II) compound $[Ni\{N(CH_2CH_2AsPh_2)_3\}Ph](BPh_4)$.[31] Lastly, extended Hückel calculations[32] based on the crystallographic structure of $[Ni(psnet)]^+$ substantiate the ground state configuration $...(d_{z^2})^1$. The HOMO is a $\sigma^*$ orbital 2.32 eV above the last filled d-type MO. Its metal component is nearly entirely $3d_{z^2}$ (33%; 2% $4p_y$) with significant contributions from phosphorus (10%) and sulfur (39%). The nitrogen component is 4%; all other contributions are <1%.

**Dihydrogen Evolution Reactions.** With $[Ni(psnet)]^+$ established as an authentic Ni(I) complex of known structure, ground state, and redox capacity, its reactions with Bronsted acids were next investigated. Previously, stoichiometric dihydrogen evolution from Ni(II) hydrides[7] and boron hydrides[33] in the presence of acids had been documented. Three monohydride sources, $NaBH(OMe)_3$, $[Ni(diphos)H](BF_4)$,[20] and $[Ni(NS_3{}^{tBu})H](BPh_4)$[19] were chosen as primary standards for the purposes of verifying the efficacy of the $H_2$ quantitation procedure and probing the proton-reducing ability of well-characterized Ni(II) hydrides. With reference to Table 3, reaction of all three compounds with excess strong acid produces ≥90% yields of dihydrogen. For the two Ni(II) complexes, dihydrogen is evolved in reactions 3 and 4, minimally represented as reaction 5. When one equivalent of $HBF_4{\cdot}Et_2O$ was used, $[Ni(diphos)_2](BF_4)_2$ was isolated in quantitative yield from a large-scale reaction. When reaction 4 was conducted with 1 equiv of ethereal HCl, the known product chloride complex[19] was formed in an in situ yield of 84% determined spectrophotometrically. With this demonstration of high-yield stoichiometric protonations of nickel(II) hydrides, attention was directed to the mediation of dihydrogen formation by an initial Ni(I) reactant.

**Table 3.** Yields of Dihydrogen Evolution Reactions

| compound | acid | equiv $H^+$ | solvent | time[a] | % yield $H_2$[b] |
|---|---|---|---|---|---|
| $[Ni(psnet)](BF_4)$ | $HBF_4{\cdot}Et_2O$[c] | 8 | DMF | *d* | <5 |
| | | 1 | PC | 5 min | 91 |
| | | 8 | PC | *d* | 55 |
| | $HCl/Et_2O$[e] | 1 | DMF | 120 min | 88 |
| | | 8 | DMF | 45 min | 90 |
| | | 8 | PC | 45 min | 92 |
| | aq HCl[f] | 8 | DMF | 24 h | 86 |
| | | 8 | PC | 12 h | 94 |
| | aq HBr[f] | 8 | DMF | *d* | 61 |
| | | 8 | PC | 12 h | 95 |
| | aq HI[f] | 8 | DMF | *d* | 57 |
| | | 8 | PC | 6 h | 94 |
| | aq $H_2SO_4$[f] | 8 | DMF | *d* | 51 |
| | | 8 | PC | 24 h | 97 |
| standards | | | | | |
| $NaHB(OMe)_3$ | aq HCl | 8 | THF | 30 min | 97 |
| $[Ni(diphos)_2H](BF_4)$ | $HBF_4{\cdot}Et_2O$ | 1 | $CH_2Cl_2$ | 2 h | 87 |
| | | 8 | $CH_2Cl_2$ | 30 min | 94 |
| $[Ni(NS_3{}^{tBu})H]BPh_4$ | $HCl/Et_2O$ | 1 | THF | 1 h | 85 |
| | | 8 | THF | 15 min | 90 |

[a] Approximate times at which maximum yields were obtained. For times ≤1 h, gas samples were removed at 5, 15, 30, 45, 60, and 120 min; for longer reactions, gas samples were removed every 6 h. [b] Yield basis: $1H_2/2Ni$ for $[Ni(psnet)]^+$, 1 $H_2$/1 BH or 1 Ni for standards. [c] 85%, used as the neat liquid. [d] Several days for low-yield reactions. [e] 1.0 M HCl in ether. [f] 1.0 M aqueous acid.

$$[Ni(diphos)_2H]^+ + HBF_4 \rightarrow H_2 + [Ni(diphos)_2](BF_4)_2 \quad (3)$$

$$[Ni(NS_3{}^{tBu})H]^+ + HCl \rightarrow H_2 + [Ni(NS_3{}^{tBu})Cl]^+ \quad (4)$$

$$Ni^{II}-H^- + H^+ \rightarrow Ni^{II} + H_2 \quad (5)$$

Under appropriate conditions determined empirically, $[Ni(psnet)]^+$ reacts with ethereal HCl, $HBF_4{\cdot}Et_2O$, and aqueous HCl, HBr, HI, and $H_2SO_4$ to yield dihydrogen (Table 3). The rate of $H_2$ production is highly dependent on the acid used, with nonaqueous acids reacting much faster than aqueous acids in DMF and PC solutions. For example, 1 equiv of $HBF_4{\cdot}Et_2O$ reacts almost instantaneously with $[Ni(psnet)]^+$ in PC, causing a color change from green to purple and affording a 91% yield of $H_2$ based on the overall stoichiometry of reaction 6.

$$Ni^I + H^+ \rightarrow Ni^{II} + {}^1/_2H_2 \quad (6)$$

Similarly, ethereal HCl gave yields of 88−92% in 45 min or less. In contrast, maximum $H_2$ production with aqueous acids (used in excess) is reached after some hours. Under constant conditions, the rate of $H_2$ evolution with hydrohalic acids stands in the order of aqueous acid strength.

Interestingly, certain other strong acids, such as *p*-toluenesulfonic acid in DMF and aqueous $HNO_3$ and $HBF_4$ in DMF, produce no $H_2$ after incubation with $[Ni(psnet)]^+$ for over 72 h. As shown spectrophotometrically, *p*-toluenesulfonic acid quantitatively oxidizes $[Ni(psnet)]^+$ to $[Ni(psnet)]^{2+}$ within minutes. Nitric acid causes a slow color change from green to brown, but we could not identify the reaction product. Aqueous $HBF_4$ shows no reaction with $[Ni(psnet)]^+$ in DMF.

The nickel-containing products of all protonation reactions tested are EPR-silent, identifying them as Ni(II) species. As

(30) Maki, A. H.; Edelstein, N.; Davison, A.; Holm, R. H. *J. Am. Chem. Soc.* **1964**, *86*, 4580.
(31) Sacconi, L.; Dapporto, P.; Stoppioni, P. *Inorg. Chem.* **1976**, *15*, 325.
(32) Extended Hückel calculations employed the program CACAO (PC version 4.0): Mealli, C.; Proserpio, D. M. *J. Chem. Educ.* **1990**, *67*, 399. In these calculations, the *z*-axis is in the Ni−S direction and the *x*-axis in the Ni−N direction. Parameters: (a) Summerville, R. H.; Hoffmann, R. *J. Am. Chem. Soc.* **1976**, *98*, 7240. (b) Lauher, J. W.; Elian, M.; Summerville, R. H.; Hoffmann, R. *J. Am. Chem. Soc.* **1976**, *98*, 3219. (c) Chen, M. M. L.; Hoffmann, R. *J. Am. Chem. Soc.* **1976**, *98*, 1647.
(33) (a) Brown, H. C.; Schlesinger, H. I.; Sheft, I.; Ritter, D. M. *J. Am. Chem. Soc.* **1953**, *75*, 192. (b) Cotton, F. A.; Wilkinson, G. *Advanced Inorganic Chemistry*, 5th ed.; Wiley-Interscience: New York, 1988, Chapter 6.

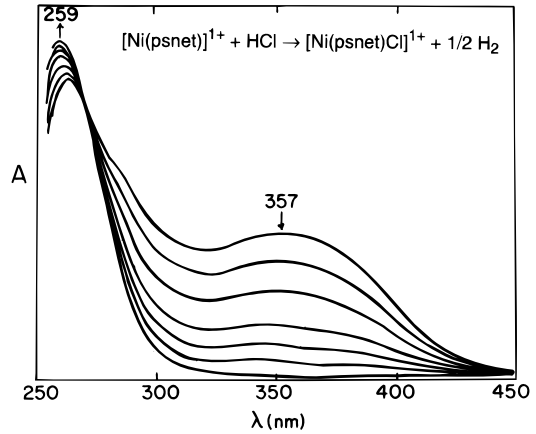


**Figure 7.** Spectrophotometric display of the time course of a reaction system in DMF initially 1.05 mM in $[Ni(psnet)]^+$ and 25 mM in HCl. The spectra were recorded over 1 h; band maxima and an isosbestic point are indicated.

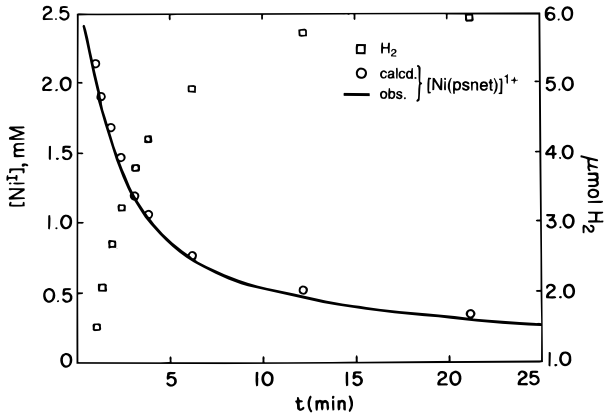


**Figure 8.** Time course of the consumption of $[Ni(psnet)]^+ = Ni(I)$ and production of $H_2$ in a reaction system in DMF initially 2.67 mM in Ni(I) and 30 mM in HCl: □, micromoles of $H_2$ determined by GC; ○, [Ni(I)] calculated from $H_2$ yields under the stoichiometry of reaction 6. The solid line is [Ni(I)] determined spectrophotometrically.

determined spectrophotometrically, reaction of $[Ni(psnet)]^+$ with 1 equiv of $HBF_4{\cdot}Et_2O$ in PC produces $[Ni(psnet)]^{2+}$ in 90% yield. Further, when 1−20 equiv of ethereal HCl are used in DMF solution, $[Ni(psnet)Cl]^+$ is formed in 89−94% yields. The reaction products were additionally identified by FAB-MS. The solution structures of Ni(II) products formed in other reaction systems (Table 3) were not determined.

**Kinetics of Dihydrogen Evolution.** We have noted above several minimal pathways that have been proposed for the reduction of protons by low-valent nickel complexes. However, no detailed mechanistic investigation of nickel-based proton reduction with fully characterized reactants and products has been reported. Given the finding that several protic sources react with $[Ni(psnet)]^+$ to produce $H_2$ according to the stoichiometry of reaction 6, these $H_2$ evolution systems based on protonation of $[Ni(psnet)]^+$ present an excellent opportunity for such an investigation.

**(a) Selection of Reaction System.** The system $[Ni(psnet)]^+$/ethereal HCl in DMF has been selected for kinetics analysis. Its reaction is essentially quantitative (Table 3) and proceeds at a rate convenient for spectrophotometric monitoring. On the basis of a much faster reaction rate and lower $H_2$ yield with excess acid, the system with $HBF_4{\cdot}Et_2O$ as the protic source in PC is considerably less attractive. Systems containing aqueous acids in DMF or PC solvent are not optimal, given the sensitivity of acid dissociation constants in nonaqueous media to small fluctuations in water content;[34] these constants may enter into a kinetics analysis (vide infra). Finally, DMF was chosen over PC as the solvent because quantitative chloride binding in $[Ni(psnet)Cl]^+$ was not observed in the latter. Solutions of [Ni(psnet)Cl]Cl in PC invariably contain mixtures of low-spin $[Ni(psnet)]^{2+}$ and high-spin $[Ni(psnet)Cl]^+$, thereby complicating the absorption spectra. All observations hereafter refer to the reaction system $[Ni(psnet)]^+$/1.0 M HCl in $Et_2O$/DMF.

**(b) Intermediates.** Several reactions were performed by incubating $[Ni(psnet)]^+$ (*ca.* 1 mM) with excess acid in an EPR tube at −10 to −40 °C for 5 s to 5 min followed by immersion in liquid nitrogen. In all cases, the EPR spectrum of unreacted $[Ni(psnet)]^+$ exhibited diminished intensity compared with the initial solution, and no other signals were observed. While not detecting an odd-spin intermediate, the procedure is slow and the possibility of a short-lived $Ni^{III}-H^-$ intermediate remains open.

**(c) Time Course of $H_2$ Evolution.** Spectral changes at 250−450 nm accompanying the reaction of $[Ni(psnet)]^+$ with ethereal HCl are depicted in Figure 7. The feature of $[Ni(psnet)]^+$ at 357 nm diminishes, while the band at 259 nm due to $[Ni(psnet)Cl]^+$ increases in intensity as the reaction proceeds. A clean isosbestic point is observed at 272 nm, indicating negligible accumulation of intermediates. The final UV−visible spectrum is identical with that of authentic $[Ni(psnet)Cl]^+$ (Figure 3).

Presented in Figure 8 are the time courses for $H_2$ production (determined by GC) and $[Ni(psnet)]^+$ consumption (monitored spectrophotometrically) in a typical reaction. Both sets of points are derived from the reactions performed with the same DMF stock solution of $[Ni(psnet)]^+$. Also shown is a plot of $[Ni(psnet)]^+$ concentration as calculated from $H_2$ yields assuming the stoichiometry of reaction 6. The near-coincidence of calculated and observed Ni(I) concentrations indicates that $H_2$ evolution tracks very closely with Ni(I) consumption, from which we conclude that *$H_2$ production is directly coupled to Ni(I) oxidation*. For both the observed and calculated values of $[Ni^I]$, plots of $1/[Ni^I]$ vs time are linear to three half-lives, showing that both data sets support kinetics second order in Ni(I) (vide infra).

**(d) HCl Equilibria in DMF.** Reported values for the $pK_a$ of HCl in DMF occur in the range 1.4−3.6.[34] The water content of the solvent used in the determination of these constants varied from 5 mM ($pK_a = 3.2-3.6$) to 100 mM ($pK_a = 1.4$). Because $pK_a$ values in nonaqueous media may vary significantly according to solvent preparation and water content,[34] we have redetermined the dissociation constant of HCl in the DMF solvent lot used for kinetics measurements. In addition to the intrinsic acidity of reaction 7, Kolthoff *et al.*[35] have shown that

$$HCl \rightleftharpoons H^+ + Cl^- \qquad K_a \tag{7}$$

$$2HCl \rightleftharpoons H_2Cl_2 \rightleftharpoons H^+ + HCl_2^- \tag{8}$$

$$HCl + Cl^- \rightleftharpoons HCl_2^- \qquad K_f \tag{9}$$

the acidity of HCl in DMF solutions is influenced by the homoconjugation equilibrium 8. They estimated the formation constant of $HCl_2^-$ in reaction 9 to fall in the range 100−200 $M^{-1}$. Equilibrium constants $K_a$ and $K_f$ are implicated in the kinetics analysis that follows.

The equilibrium constants for dissociation and homoconjugation of HCl in DMF were determined conductimetrically in

(34) Izutsu, K. *Acid-Base Dissociation Constants in Dipolar Aprotic Solvents*; IUPAC Chemical Data Series No. 35; Blackwell Scientific: Oxford, U.K., 1990.
(35) Kolthoff, I. M.; Chantooni, M. K., Jr.; Smagowski, H. *Anal. Chem.* **1970**, *42*, 1622.

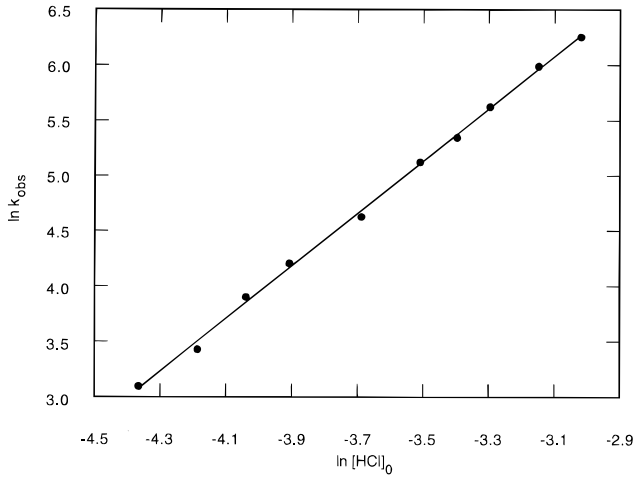


**Figure 9.** Dependence of reaction rate on the concentration of HCl at $[Ni^I] = 1.00$ mM, $[HCl]_0 = 12-49$ mM, and 25 °C. The solid line is a fit of the data to the equation $\ln k_{obs} = 12.7 + 2.18 \ln[HCl]_0$ ($R = 0.996$).

solutions that contained <5% (v/v) of ether.[36] A plot of molar conductance $\Lambda_m$ vs $[HCl]^{1/2}$ exhibited marked departure from linearity when [HCl] > 0.01 M, consistent with $HCl_2^-$ formation. From data in the regime [HCl] < $1.6 \times 10^{-3}$ M, where homoconjugation is minimal, the dissociation constant was determined to be $K_a = 1.3 \times 10^{-5}$ M ($pK_a = 4.9$). This marked increase in the $pK_a$ value compared with the cited literature values is attributed to the lower water content in the solvent lot used here (≤1.1 mM) and the presence of 0−5% (v/v) of ether. The formation constant for $HCl_2^-$ was estimated by plotting $\Lambda_m([HCl]([HCl] + 1/K_f))^{1/2}$ vs [HCl] for various values of $K_f$.[35] Linear plots were obtained for the values $K_f = 20-250$ $M^{-1}$, with the best fits obtained for $K_f = 40-80$ $M^{-1}$.

**(e) Reaction Order and Anion Effect.** The kinetics of reaction 6 ($Ni^I = [Ni(psnet)]^+$) were investigated spectrophotometrically by following the diminution of the $[Ni(psnet)]^+$ absorbance at 380 nm. Protonation reactions performed with >8 equiv of HCl exhibited clean second order kinetics with respect to Ni(I), as indicated by linear plots of $\{(A_0 - A_\infty)/(A_t - A_\infty)[Ni^I]_0\}$ vs time (not shown). Reaction rates at various HCl concentrations were determined from the slopes of these plots. Within a concentration range that gave reasonable initial absorbances of $[Ni(psnet)]^+$ (>0.42 mM), the systems displayed pseudo-second-order kinetics for $[HCl]_0/[Ni^I] = 8-100$. At the ratios $[HCl]_0/[Ni^I] \gg 100$, the reaction rates prohibited observation of the initial phase of the reaction (*ca*. 25% completion) by the method employed. The dependence of observed rates vs $[HCl]_0$ under the conditions $[HCl]_0/[Ni^I] \approx 10-50$ is shown in the logarithmic plot of Figure 9. On the basis of the relationship $\ln k_{obs} = \ln k + a \ln[HCl]_0$, the data were satisfactorily fitted with $a = 2.18$, corresponding to a reaction apparently mixed order in HCl.

The addition of chloride as $Bu_4NCl$ was found to accelerate reaction 6 dramatically. Further, the apparent reaction order in Ni(I) was found to be dependent on the added chloride concentration. Three regimes were identified: clean first-order behavior at high $[Cl^-]_0$; mixed first-order−second-order at intermediate values of $[Cl^-]_0$; clean second-order behavior at low $[Cl^-]_0$. More specifically, at $[Ni^I] = 0.42$ mM and $[Cl^-]_0$ > 30 mM, the reaction becomes first order in Ni(I) as demonstrated by linear plots of $\ln\{(A_t - A_\infty)/(A_0 - A_\infty)\}$ vs time (not shown), while, at $[Cl^-]_0$ < 1.6 mM, the reaction

(36) Method of data analysis: French, C. M.; Roe, I. G. *Trans. Faraday Soc*. **1953**, *49*, 314.

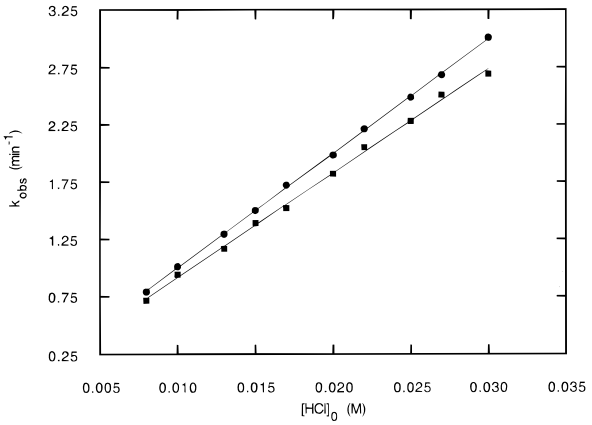


**Figure 10.** Dependence of reaction rate on the concentration of HCl at $[Ni^I] = 0.55-1.00$ mM, $[HCl]_0 = 7.5-29.5$ mM, and 25 °C. For the plot with points ●, $[Cl^-]_0 = 0.122$ M; the solid line is a fit of the data to the equation $k_{obs} = 0.0015 + 99.9[HCl]_0$ ($R = 0.999$). For the plot with points ■, $[Cl^-]_0 = 0.090$ M; the solid line is a fit of the data to the equation $k_{obs} = 0.0018 + 91.3[HCl]_0$ ($R = 0.998$).

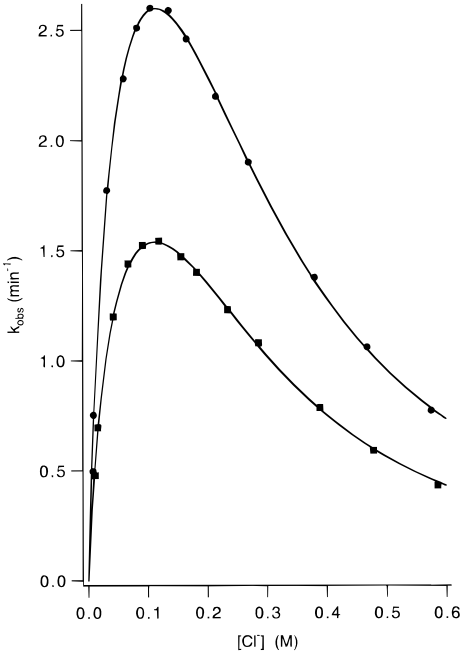


**Figure 11.** Dependence of reaction rate on the concentration of $[Bu_4NCl]$ at $[Ni^I] = 0.42-0.55$ mM, $[Bu_4NCl]_0 > 30$ mM, and 25 °C. For the plot with points ●, $[HCl]_0 = 25$ mM; the solid line is a fit of the data to the equation $k_{obs} = 91.8[Cl^-]/\{(1 + 0.26[Cl^-] + 12.1[Cl^-]^2)(1 + 21[Cl^-])\}$. For the plot with points ■, $[HCl]_0 = 15$ mM; the solid line is a fit of the data to the equation $k_{obs} = 56.3[Cl^-]/\{(1 + 0.28[Cl^-] + 12.1[Cl^-]^2)(1 + 22[Cl^-])\}$.

exhibits a second-order dependence on Ni(I). In the regime $[Cl^-]_0 > 30$ mM, the reaction becomes first order in HCl, as demonstrated by the linear plots in Figure 10. When $[HCl]_0$ is held constant, the rate exhibits the complex bell-shaped dependence on $[Cl^-]$ shown in Figure 11. When $[HCl]_0$ was varied at constant $[Bu_4NPF_6] = 0.125$ M, the data were satisfactorily fitted to the equation given above for Figure 9 with $a = 2.09$ (not shown), consistent with either a second-order or mixed-order reaction.

To examine the anion effect further, reactions were performed at various concentrations of $(Bu_4N)(PF_6)$ in the presence and absence of $Bu_4NCl$. In the latter case, second-order kinetics in Ni(I) were observed. In the presence of both salts, a mixed-order dependence in Ni(I) was found under conditions where first-order dependence applies in the absence of $(Bu_4N)(PF_6)$. A plot of the observed reaction rate vs $[Bu_4NPF_6]$ in the absence

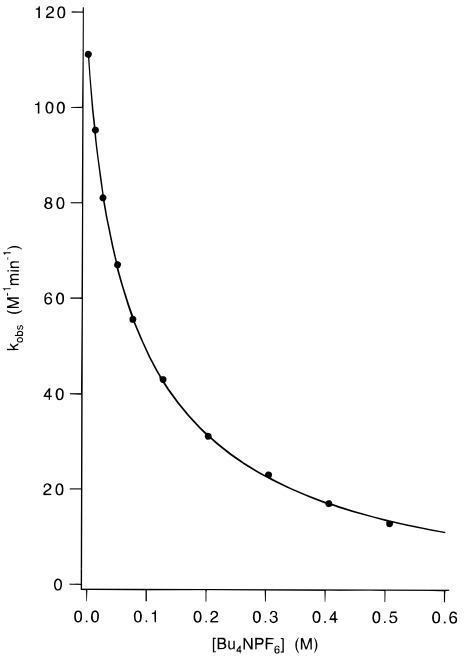


**Figure 12.** Dependence of reaction rate on the concentration of $(Bu_4N)(PF_6)$ at $[Ni^I] = 0.55$ mM, $[HCl]_0 = 25$ mM, $[Bu_4NPF_6] = 0-0.5$ M, and 25 °C. The solid line is a fit of the data to the equation $k_{obs} = (10.6 + 130.7[Bu_4NPF_6])^2/(1 + 19.9[Bu_4NPF_6] + 38.2[Bu_4NPF_6]^2)^2$.

of added chloride (second order in Ni(I)) is presented in Figure 12. The $PF_6^-$ anion slows the reaction markedly compared to systems in which $[Ni(psnet)](BF_4)$ and HCl are the only sources of anions.

The influence of anion concentration on the rate of reaction 6 cannot be adequately explained by a general effect of ionic strength on the nature of the reaction medium. Such a model would predict a monotonic increase or decrease in reaction rate as a function of anion concentration for both $Cl^-$ and $PF_6^-$.[37] The quadratic dependence of $[Cl^-]$ contradicts this prediction. Also, the change from first-order kinetics in Ni(I) at high $[Cl^-]/[PF_6^-]$ to second-order behavior at low concentration ratios suggests that a specific nickel−anion interaction occurs in the rate-determining step. Given the propensity of charged species to form ion pairs in nonaqueous media, the data strongly imply that *specific* nickel−chloride ion pair(s) are responsible for the observed chloride effect. The rate-retarding effect of $(Bu_4N)(PF_6)$ at high $[PF_6^-]/[Cl^-]$ may be attributed to the displacement of $Cl^-$ with $PF_6^-$ in the ion pair.

**(f) Rate Law and Proposed Mechanism.** The overall reaction 6 can be variously formulated in terms of coupled elementary reactions, such as the minimal steps of eq 2a,b. These may include metal protonation, electron transfer, hydride protonation, and bimolecular collapse of two $Ni^{III}-H^-$ species. In the systems at hand, other elementary steps including ligand dissociation, ligand protonation, chloride binding, and ion pairing were considered. Various combinations of elementary steps have been formulated, and the rate law for each has been derived under the rapid-equilibrium or steady-state approximation. The number of possible reaction sets is too large for a full description. We begin with that shown in Scheme 1, which fits satisfactorily all experimental data, and subsequently show that two other seemingly viable schemes do not. For simplicity,

(37) Moore, J. W.; Pearson, R. G. *Kinetics and Mechanism*; Wiley: New York, 1981; Chapter 7.

**Scheme 1**

$$Ni(I)^+ + H^+ \underset{k_{-1}}{\overset{k_1}{\rightleftharpoons}} Ni{-}H^{2+} \quad (10)$$

$$Ni{-}H^{2+} + 2Cl^- \underset{k_{-2}}{\overset{k_2}{\rightleftharpoons}} Ni{-}H^{2+}|Cl^- + Cl^- \underset{k_{-3}}{\overset{k_3}{\rightleftharpoons}} Ni{-}H^{2+}|2Cl^- \quad (11)$$

**A**

$$Ni{-}H^{2+}|Cl^- \underset{k_{-4}}{\overset{k_4}{\rightleftharpoons}} Ni{-}(H)Cl^+ \quad (A1)$$

$$Ni{-}H^{2+}|2Cl^- \underset{k_{-5}}{\overset{k_5}{\rightleftharpoons}} Ni{-}(H)Cl^+|Cl^- \quad (A2)$$

$$2Ni{-}(H)Cl^+ \xrightarrow{k_6} 2Ni{-}Cl^+ + H_2 \quad (A3)$$

$$2Ni{-}(H)Cl^+|Cl^- \xrightarrow{k_7} 2Ni{-}Cl^+ + H_2 + 2Cl^- \quad (A4)$$

$$Ni{-}(H)Cl^+ + Ni{-}(H)Cl^+|Cl^- \xrightarrow{k_8} 2Ni{-}Cl^+ + H_2 + 2Cl^- \quad (A5)$$

(A3)–(A5): rate-limiting step

**B**

$$Ni{-}H^{2+}|2Cl^- \xrightarrow{k_9} Ni{-}(H)Cl_2 \quad \text{rate-limiting step} \quad (B1)$$

$$2Ni{-}(H)Cl_2 \longrightarrow 2Ni{-}Cl^+ + H_2 + 2Cl^- \quad (B2)$$

or electron transfer

$$Ni{-}(H)Cl_2 + Ni(I)^+ \longrightarrow Ni{-}(H)Cl_2^- + Ni(II)^{2+} \quad (B3)$$

$$Ni(H)Cl_2^- + H^+ \longrightarrow Ni{-}Cl^+ + H_2 + Cl^- \quad (B4)$$

$$Ni(II)^{2+} + Cl^- \longrightarrow Ni{-}Cl^+ \quad (B5)$$

the species in Scheme 1 do not carry oxidation states (e.g., $Ni-H^{2+} = Ni^{III}-H^-$).[38]

The most reasonable initial step is protonation of the Ni(I) center, as in eq 10. The product dication reacts with 1 or 2 equiv of chloride in eq 11 to form the corresponding ion pairs. The concentrations of these species (and their reaction products) in different $[Cl^-]$ regimes dictate the chloride-dependent effects on rate and reaction order. Following their formation, two reaction pathways A and B promote $H_2$ production, with path A prevailing at low chloride concentrations and path B at high chloride concentrations.

**Path A.** Both the mono- and dichloride ion pairs collapse to bound nickel(III) chloride−hydride species (reactions A1 and A2). (Given the metal oxidation state, one or both phosphine groups are likely to decoordinate to maintain a coordination number ≤ 6.) Subsequent rate-determining reaction of two such species in the three possible combinations (reactions A3−A5) affords $H_2$, $Ni^{II}-Cl^-$, and free chloride in two cases. These steps correspond to minimal reaction 2b.

**Path B.** At high chloride concentration, the *di*chloride ion pair undergoes rate-determining collapse with partial ligand decoordination to a bound nickel(III) hydride−dichloride (reaction B1). Thereafter, $H_2$ formation can occur bimolecularly (reaction B2, an elaboration of reaction 2b) or by an electron-transfer sequence (reactions B3−B5); these routes cannot be distinguished past the rate-determining step. Derivations of the rate laws in the sections which follow are outlined in the Appendix.

The two-term rate law corresponding to the reactions in Scheme 1 is given by eq 12; $K_n = k_n/k_{-n}$ ($n = 1-5$). Several simplifying assumptions have been made in its derivation. Following protonation reaction 10, the ion pair equilibria of eq 11 are established immediately, such that the $Ni-H^{2+}$ concentration before reaction can be expressed as a sum of the concentrations of the three hydride species. The ion-pair status of such species does not importantly influence the rate of their bimolecular collapse to form $H_2$ and $Ni-Cl^+$ ($k_6 = k_7 = k_8$). The first and second terms describe the reaction order at low

(38) In the notation of Schemes 1−4, a vertical line signifies an ion pair, with the species to the right of the line uncoordinated (e.g., $Ni-H^{2+}|Cl^-$ = nickel(III)−hydride chloride 1:1 ion pair). The absence of a vertical line implies that all species are coordinated (e.g., $Ni-(H)Cl_2$ = nickel(III)−hydride/bis chloride complex (requiring some decoordination of the psnet ligand)).

$$-\frac{d[Ni^I]}{dt} = k_6 K_a^{\,2} K_1^{\,2}(K_2K_4 + K_a^{\,1/2}K_2K_3K_5[HCl]_0^{\,1/2})^2[Ni^I]^2[HCl]_0^{\,2} + \frac{k_9 K_a K_1 K_2 K_3 [Cl^-][Ni^I][HCl]_0}{(1 + K_2[Cl^-] + K_2K_3[Cl^-]^2)(1 + K_f[Cl^-])} \quad (12)$$

and high chloride concentrations, respectively. The first term does not contain the chloride dependence present in the more general expression (eq 9A, Appendix) because its contribution at low $[Cl^-]$ is negligible.

At intermediate chloride concentrations, a combination of the two terms accounts for the observed rate profile (vide infra). The first term predicts second-order behavior in Ni(I) with HCl as the only chloride source. It further anticipates the apparent noninteger order in HCl described in Figure 9; expansion of the first term affords an order between 2 and 3 for this reactant. Shown in Figure 13 is a fit of the observed rate constants at varying $[HCl]_0$ to the general expression 13, where $\alpha$ and $\beta$ are products of constant $[Ni^I]$ and rate and equilibrium constants of elementary reactions appearing in the first term of eq 12.

$$k_{obs} = [HCl]_0^{\,2}(\alpha + \beta[HCl]_0^{\,1/2})^2 \quad (13)$$

The second term predicts first-order kinetics in both Ni(I) and HCl in the high-$[Cl^-]$ region, consistent with the observed reaction orders of these species. In addition, it accounts for the bell-shaped dependence of the observed rate on chloride concentration. Illustrated in Figure 11 are two fits of observed rate constants at constant $[HCl]_0$ and varying $[Cl^-]$ to the general eq 14, in which $\gamma$, $\delta$, and $\epsilon$ are constant terms.[39] Highly satisfactory fits were obtained from eqs 13 and 14, consistent with the operation of Paths A and B.

$$k_{obs} = \gamma[Cl^-]/(1 + \delta[Cl^-] + \epsilon[Cl^-]^2)(1 + K_f[Cl^-]) \quad (14)$$

The values $K_2 = 0.26-0.28\ M^{-1}$ ($\delta$) and $K_3 = 43-46\ M^{-1}$ derived from fits of the data to eq 14 indicate that formation of the neutral *di*chloride ion pair is decidedly favored over its *mono*chloride counterpart (Scheme 1). Inasmuch as the dichloride is the entry point to $H_2$ formation via path B, its preferential formation may explain why this reaction pathway begins to dominate at chloride concentrations as low as *ca*. 30 mM.

The first order dependence on HCl displayed in Figure 10 requires comment. Although the added chloride concentration is constant in a given set of experiments (0.090 or 0.122 M), homoconjugation equilibrium 9 causes the actual chloride concentration to vary (*ca*. 20%) over the range of [HCl] used. However, the term $[Cl^-]/(1 + K_2[Cl^-] + K_2K_3[Cl^-]^2/(1 + K_f[Cl^-])$ remains constant to within 2% over the range of [HCl] used at both concentrations of added chloride, leading to the observed linear dependence of rate on $[HCl]_0$.

Calculation of initial rates described by eq 12 at varying chloride concentrations confirmed that the first term controls the rate in the low chloride regime, while the second term predominates in the high chloride region. Equation 3A (Appendix) was used to calculate values of $[Cl^-]$ in experiments in which HCl was the only source of chloride. The relative values of the first and second terms are strongly influenced by the value of $K_f$ for homoconjugation reaction 9 used in the calculation, for this value modulates the chloride concentration in the numerator of the second term.

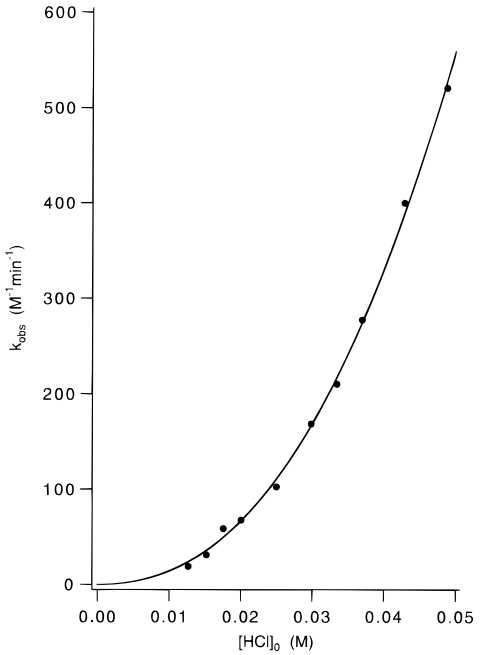


**Figure 13.** Dependence of reaction rate on the concentration of HCl at $[Ni^I] = 1.00$ mM, $[HCl]_0 = 12-49$ mM, and 25 °C. The solid line is a fit of the data to the equation $k_{obs} = [HCl]_0^{\,2}(290.4 + 817.4[HCl]_0^{\,1/2})^2$.

The rate behavior in the *intermediate* range of chloride concentration (*ca*. 1.6−30 mM), in which a mixed-order dependence on $[Ni^I]$ is observed, is most readily evaluated using the integrated form 15 of rate law 12. For this purpose, the

$$\ln([Ni^I]/(k_i[Ni^I] + k_{ii})) = -k_{ii}t + \ln([Ni^I]_0/(k_i[Ni^I]_0 + k_{ii})) \quad (15)$$

latter may be written as $-d[Ni^I]/dt = k_i[Ni^I]^2 + k_{ii}[Ni^I]$, in which the terms $k_i$ and $k_{ii}$ refer to the rate constants for the first and second terms of the rate law, respectively. Data from this concentration range were fitted to the equation $t = -1/(k_{ii}\ln([Ni^I]/(k_i[Ni^I] + k_{ii})) + C'$, using $k_i$, $k_{ii}$, and $C'$ as parameters. Values of $k_i$ and $k_{ii}$ obtained from the fits were compared with observed or calculated values of these constants. For data in the low end of the range ($[Cl^-]_0 = 1.6-3.0$ mM), $K_f[Cl^-]$ is negligible and $k_i$ is approximated by the $k_{obs}$ value for the corresponding experiment in which no chloride was added. From eq 12 we find $k_{obs} = 112\ M^{-1}\ min^{-1}$, vs $k_i = 104-114\ M^{-1}\ min^{-1}$ from the fits. Within this low range, values of $k_{ii}$ were calculated from eq 12. At higher $[Cl^-]_0$ values within the range, $k_i$ is determined by the general rate law (eq 9A, Appendix) and could not be meaningfully calculated owing to insufficient knowledge of certain constants in the equation. From the form of this equation, $k_i$ is expected to decrease slightly (*ca*. 20%) at higher $[Cl^-]_0$. Although the entire intermediate region could not be tested, the $k_i$ and $k_{ii}$ values obtained from the fits matched the expected values to within 20%. This result offers additional support for the dual path A/B mechanism of Scheme 1.

**(g) Retardation of $H_2$ Formation.** Set out in Scheme 2 is the proposed mechanism by which $PF_6^-$, taken as a noncoordinating anion in DMF solution, retards the rate of $H_2$ production in reaction 6. After the Ni(I) protonation reaction 10, all

(39) The value of $K_f$ (eq 9) used in the fits requires comment. The $[Cl^-]$ values in the second term of eq 12 correspond to concentrations after homoconjugation is considered. They were calculated using eqs 1A and 2A of the Appendix. An iterative approach in which $[Cl^-]$ was calculated from a given value of $K_f$ with $\gamma$, $\delta$, and $\epsilon$ treated as fitting parameters failed to produce a self-consistent value of $K_f$. Thereafter, eq 14 was fit for several fixed values of $K_f$ with $\gamma$, $\delta$, and $\epsilon$ as variables. Reasonable fits were obtained for $K_f = 5-25\ M^{-1}$; these values overlap those obtained by conductivity measurements in the range $20-25\ M^{-1}$. The equations plotted in Figure 11 represent the best fits to the data within this latter range of $K_f$ values.

**Scheme 2**

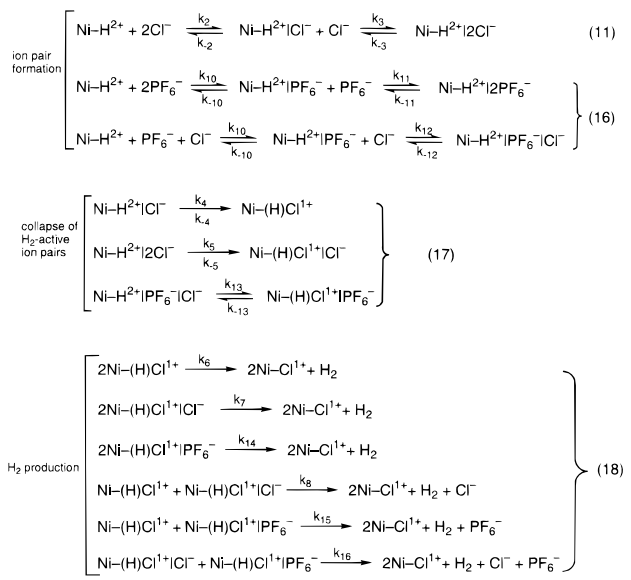


possible $Ni-Cl^{-}-PF_6^{-}$ ion pairs are formed (eqs 11 and 16). Collapse of the $Ni-Cl^{-}$ ion pairs affords three $Ni-HCl^{+}$ intermediates (eqs 17), which subsequently react in six possible combinations to form $H_2$, $Ni-Cl^{+}$, $PF_6^{-}$, and free chloride (eqs 18). These steps are equivalent to minimal reaction 2b. Rate eq 19 is derived from Scheme 2, in which all possible

$$\frac{-\mathrm{d}[\mathrm{Ni^I}]}{\mathrm{d}t} = k_6 K_a^{\,2} K_1^{\,2} [\mathrm{Ni^I}]^2 [\mathrm{HCl}]_0^{\,2} \times \left( \frac{K_2K_4 + K_2K_3K_5[\mathrm{Cl^-}] + K_{10}K_{12}K_{13}[\mathrm{PF_6^-}]}{1 + (K_{10} + K_{10}K_{12}[\mathrm{Cl^-}])[\mathrm{PF_6^-}] + K_{10}K_{11}[\mathrm{PF_6^-}]^2} \right)^2 \quad (19)$$

intermediate species are included because none can be excluded on the basis of experiment. Development of this equation involves assumptions similar to those for eq 12. The $Ni-H^{2+}$ concentrations can be written as a sum of all $Ni-PF_6^{-}-Cl^{-}$ ion pairs. The rate of $Ni-H^{2+}$ species collapse to form $H_2$ and $Ni-Cl^{+}$ is independent of ion-pair status ($k_6 = k_7 = k_8 = k_{14} = k_{15} = k_{16}$). Certain terms in $[Cl^{-}]$ present in the general expression of the rate law (eq 12A, Appendix), negligible at the low chloride concentrations used to discern the effect of $[Bu_4NPF_6]$ on rate, are omitted.

The rate law predicts second-order kinetics in Ni(I) and HCl, consistent with the reaction orders described above. Shown in Figure 12 is a fit of the observed rate constants to the general eq 20. Both of the coupled reactions of Scheme 2 and the

$$k_{obs} = (\zeta + \eta[\mathrm{Bu_4NPF_6}])^2/(1 + \theta[\mathrm{Bu_4NPF_6}] + \kappa[\mathrm{Bu_4NPF_6}]^2)^2 \quad (20)$$

derived rate law show how $PF_6^{-}$ slows the rate of $H_2$ formation. This anion competes with chloride to form nonproductive ion pairs that cannot collapse to active $Ni-HCl^{2+}$ intermediates (Scheme 1). In the development of the kinetics scheme, the observation of rate retardation by $PF_6^{-}$ and change in Ni(I) reaction order were significant for these effects suggested the intervention of ion pairing in the mechanism of $H_2$ evolution.

We interpret our data on anion effects to implicate the formation and collapse of mono- and dichloride ion pairs as prerequisite to $H_2$ formation in the $[Ni(psnet)]^{+}$/HCl/DMF system. Given the obvious preference of the Ni(III) oxidation state for hard anionic ligands,[40] chloride binding may stabilize the $Ni-H^{2+}$ intermediate as $Ni-HCl = Ni^{III}-H^{-}Cl^{-}$ or $Ni-HCl_2 = Ni^{III}-H^{-}Cl^{-}{}_2$. We have already noted that the psnet ligand alone does not stabilize Ni(III) sufficiently to afford a reversible $[Ni(psnet)]^{2+,3+}$ couple. Decoordination of phosphine groups would effect a coordination number of 6 or less in chloride-bound species and would also lessen steric congestion and thus facilitate bimolecular reactions of the $Ni-HCl^{+}$ intermediate in steps A3−A5 of path A. Collapse of the dichloride ion pair to $Ni-HCl_2$ is expected to engender the rate enhancement observed in the presence of exogenous chloride. Binding of two chlorides to the nickel(III)−hydride necessitates the displacement of both phosphine groups to maintain a reasonable coordination number. The energy required to decoordinate the two groups may explain why collapse of the ion pair in reaction B1 could be rate-limiting in path B. Bimolecular reaction B2 could be enhanced as a result of decreased steric hindrance at the Ni(III) center. However, opening up of the coordination sphere could also enhance the rate of reaction B3 by chloride-bridged inner-sphere electron transfer, resulting in $H_2$ formation by steps B3 and B4. As noted above, we cannot resolve path B after the rate-determining step.

**Related Steps in $H_2$ Formation in Other Systems.** The protonation of low-valent metals to form metal hydrides, followed in some cases by $H_2$ evolution upon reaction with additional protons, is precedented for a number of transition metals. The situation has been most recently summarized by Koelle.[41] Of particular relevance to the system at hand are the reactivities of certain cobalt−hydride complexes. Thus $[HCo(CN)_5]^{3-}$ evolves $H_2$ in bimolecular reaction 21,[42] analogous to

$$2[\mathrm{HCo(CN)_5}]^{3-} \rightarrow \mathrm{H_2} + 2[\mathrm{Co(CN)_5}]^{3-} \quad (21)$$

$$[\mathrm{HCo(dmgH)_2(B)}] + \mathrm{H_3O^+} \rightarrow \mathrm{H_2} + [\mathrm{Co(dmgH)_2(B)(OH_2)}] \quad (22)$$

$$[\mathrm{Co^I(dmgBF_2)_2}]^- + \mathrm{H^+} \rightarrow [\mathrm{HCo^{III}(dmgBF_2)_2}] \quad (23a)$$

$$2[\mathrm{HCo^{III}(dmgBF_2)_2}] \rightarrow \mathrm{H_2} + [\mathrm{Co^{II}(dmgBF_2)_2}] \quad (23b)$$

$$[\mathrm{HCo^{III}(dmgBF_2)_2}] + \mathrm{H^+} \rightarrow \mathrm{H_2} + [\mathrm{Co^{III}(dmgBF_2)_2}]^+ \quad (23c)$$

steps A3−A5 and B2 (Scheme 1). Decomposition of a hydridocobaloxime complex was found to proceed in part by the heterolytic pathway 22 (B = base).[43] Further, cobalt-catalyzed evolution of $H_2$ has been obtained by a reaction sequence very probably including the fast reactions 23.[44] The relationship of these reactions to those in Scheme 1 and minimal reactions 2 is evident. In reaction 23c, hydride protonation precedes electron transfer, a possible sequence noted for reaction 2a and the reverse of reactions B3 and B4. All of these reactions were carried out in aqueous solution, where ion pairing is an improbable influence on the kinetics.

**Other Reaction Pathways.** Schemes 3 and 4 illustrate two simpler alternative routes to $H_2$ formation with a common initial step of Ni(I) protonation, reaction 10. In Scheme 3, $H_2$ is

(40) (a) Nag, K.; Chakravorty, A. *Chem. Rev.* **1980**, *33*, 87. (b) Lappin, A. G.; McAuley, A. *Adv. Inorg. Chem.* **1988**, *32*, 241.
(41) Koelle, U. *New J. Chem.* **1992**, *16*, 157.
(42) (a) Halpern, J.; Pribanić, M. *Inorg. Chem.* **1970**, *9*, 2616. (b) Halpern, J. *Inorg. Chim. Acta* **1983**, *77*, L105. (c) Mooiman, M. B.; Pratt, J. M. *J. Mol. Catal.* **1984**, *27*, 367.
(43) Chao, T.-H.; Espenson, J. H. *J. Am. Chem. Soc.* **1978**, *100*, 129. dmgH = dimethylglyoximate(1−).
(44) Connolly, P.; Espenson, J. H. *Inorg. Chem.* **1986**, *25*, 2684. $dmgBF_2$ = difluoroboryl dimethylglyoximate(1−).

**Scheme 3**

$$Ni(I)^+ + H^+ \underset{k_{-1}}{\overset{k_1}{\rightleftharpoons}} Ni\text{–}H^{2+} \qquad (10)$$

$$2Ni\text{–}H^{2+} \xrightarrow{k_{17}} 2Ni^{2+} + H_2 \qquad (2b)$$

$$Ni^{2+} + Cl^- \longrightarrow Ni\text{–}Cl^{1+}$$

$$-\frac{d[Ni^I]}{dt} = k_{17}[Ni\text{–}H^{2+}]^2 = k_{17}K_1[Ni^I]^2(K_a[HCl]_0 + K_aK_f[HCl]_0^2) \qquad (24)$$

**Scheme 4**

$$Ni(I)^+ + H^+ \underset{k_{-1}}{\overset{k_1}{\rightleftharpoons}} Ni\text{–}H^{2+} \qquad (10)$$

$$\left.\begin{aligned} Ni\text{–}H^{2+} + Ni^+ &\xrightarrow{k_{18}} Ni\text{–}H^{1+} + Ni^{2+} \\ Ni\text{–}H^{1+} + H^+ &\longrightarrow Ni^{2+} + H_2 \end{aligned}\right\} \quad (2a)$$

$$Ni^{2+} + Cl^- \longrightarrow Ni\text{–}Cl^{1+}$$

$$-\frac{d[Ni^I]}{dt} = k_{18}[Ni^I][Ni\text{–}H^{2+}] = k_{18}K_1[Ni^I]^2(K_a[HCl]_0 + K_aK_f[HCl]_0^2)^{1/2} \qquad (25)$$

produced by the coupling of two nickel(III) hydrides, as in minimal reaction 2b, without the formation of nickel chloride ion pairs or nickel hydride−chloride intermediates. In Scheme 4, the reaction proceeds by electron transfer between the Ni(I) reactant and the nickel(III) hydride intermediate, followed by protonation of the nickel(II) hydride, again without formation of ion pairs. This scheme is composed of the minimal reactions 2a. The derived rate laws for these schemes are eqs 24 and 25. Having related forms, neither can account for all observed reaction orders or the rate-reducing effect of $(Bu_4N)(PF_6)$. Similar limitations were encountered for all other reaction sets surveyed except those in Schemes 1 and 2.

**Summary.** The following are the principal results and conclusions of this investigation.

1. The diamagnetic complex $[Ni(psnet)]^{2+}$ is readily prepared and can be reduced electrochemically or chemically to $[Ni(psnet)]^+$; both complexes were isolated as $BF_4^-$ salts and display distorted trigonal bipyramidal structures.

2. Structural distortions relative to $[Ni(psnet)]^{2+}$ and EPR properties demonstrate that $[Ni(psnet)]^+$ is an authentic Ni(I) complex with a $...(d_{z^2})^1$ ground state.

3. In the presence of one or more equivalents of strong acid, the well-characterized Ni(II) hydrides $[Ni(diphos)_2H]^+$ and $[Ni(NS_3{}^{tBu})H]^+$ give essentially quantitative yields of $H_2$ based on the stoichiometry $Ni^{II}\text{–}H^- + H^+ \rightarrow Ni^{II} + H_2$ (eq 5), thereby demonstrating protonation of nickel-bound hydride.

4. Under appropriate conditions, $[Ni(psnet)]^+$ reacts with a series of strong acids in aprotic media to produce $H_2$, in some cases in >90% yield. Dihydrogen production was demonstrated to be directly coupled to Ni(I) oxidation under the stoichiometry $Ni^I + H^+ \rightarrow Ni^{II} + {}^1/_2H_2$ (eq 6).

5. From these results in (4), the system $[Ni(psnet)]^+$/1.0 M HCl in $Et_2O$/DMF, which affords ≳90% $H_2$ yields, was selected for a study of reaction kinetics and mechanism.

6. The system in (5) evolves $H_2$ by two parallel pathways determined by the chloride concentration and described by a two-term rate law (eq 12); $H_2$ formation is stimulated by added chloride (as $Bu_4NCl$) and retarded by added $(Bu_4N)(PF_6)$ in the overall reaction 26. At low chloride concentration, the rate exhibits a second-order dependence on $[Ni^I]$ and a non-integer dependence on $[HCl]_0$ between second and third order. At high chloride concentration the rate exhibits the first-order behavior $[Ni^I][HCl]_0$ with a quadratic dependence on $[Cl^-]$.

$$[Ni^I(psnet)]^+ + HCl \rightarrow [Ni(psnet)Cl]^+ + {}^1/_2H_2 \qquad (26)$$

7. The mechanism of reaction 26 is interpreted in terms of two sets of reactions (Scheme 1); the initial metal-centered protonation step $Ni^I + H^+ \rightarrow Ni^{III}\text{–}H^-$ is common to both. In the low $[Cl^-]$ regime, path A involves formation and collapse of ion pairs, with the rate-determining step being the minimal bimolecular reaction $2Ni^{III}\text{–}H^- \rightarrow H_2 + 2Ni^{II}$ (eq 2b). In the high $[Cl^-]$ regime, path B implicates the rate-determining collapse of a dichloride ion pair to $Ni^{III}\text{–}H^-Cl^-_2$ with attendant partial decoordination of the psnet ligand (most likely the diphenylphosphino groups). Because these paths fit all kinetics data satisfactorily, including the rate-decelerating effect of $PF_6^-$ (described by eq 19), and no other schemes satisfactory in this respect could be devised, paths A and B are taken as the most probable descriptions of overall reaction 26.

**Hydrogenase in Context.** This investigation of Ni−mediated $H_2$ formation has been motivated by the unknown reaction pathway of [NiFe] hydrogenases. While there is substantial spectroscopic information pointing toward an intimate involvement of nickel in catalysis,[1,2,45−50] the role of iron in influencing the electronic and reactivity properties of the enzymes is presently unknown. As emphasized at the outset, the system studied here cannot be a close model of the enzyme active site. The pentadentate molecule psnet is not wholly a simulator of ligand binding in a protein, the complexes $[Ni(psnet)]^{2+,1+}$ lack a bridged Ni−Fe center recently discovered in the crystal structure of *D. gigas* hydrogenase,[17] and the existence of anion effects in enzymatic proton reduction is problematic. Given the complexity of Ni-mediated $H_2$ formation, at least in terms of alternative pathways, we are less concerned with fidelity to native coordination at this stage of the problem than with demonstration of the protic reaction chemistry of a fully characterized Ni(I) molecule. This investigation has shown that an authentic mononuclear Ni(I) complex of known structure and a mildly negative redox potential can stoichiometrically evolve $H_2$ from protic sources. The reaction paths considered most probable on the basis of kinetics analysis involve steps of protic oxidative addition to Ni(I) to generate $Ni^{III}\text{–}H^-$ and, in one version of path B, electron transfer to Ni(III) followed by protonation of bound hydride to afford $H_2$. The last of these steps has been independently demonstrated (eqs 3 and 4). These events are all found in Figure 1 depicting a minimal scheme for enzymic $H^+/H_2$ interconversion. Note that hydrogenases catalyze the isotope exchange reaction $D_2O + H_2 \rightleftarrows HDO + HD$, indicating that $H_2$ is cleaved heterolytically and emphasizing the probability of a hydride intermediate, which has been widely proposed.[1]

The formation of $H_2$ by the coupling of two nickel(III) hydrides (path A) and the effect of anions on reaction rates are presumably artifacts of the synthetic system. In synthetic systems, it is often difficult to separate metal centers sufficiently to avoid nonphysiological bimolecular reactions while maintaining other design features essential to reactivity, such as open coordination sites for substrate binding and stereochemical

(45) Scott, R. A.; Wallin, S. A.; Czechowski, M.; DerVartanian, D. V.; LeGall, J.; Peck, H. D., Jr.; Moura, I. *J. Am. Chem. Soc.* **1984**, *106*, 6864.
(46) Fan, C.; Teixeira, M.; Moura, J.; Moura, I.; Huynh, B.-H.; LeGall, J.; Peck, H. D., Jr.; Hoffman, B. M. *J. Am. Chem. Soc.* **1991**, *113*, 20.
(47) (a) Barondeau, D. P.; Roberts, L. M.; Lindahl, P. A. *J. Am. Chem. Soc.* **1994**, *116*, 3442. (b) Roberts, L. M.; Lindahl, P. A. *Biochemistry* **1994**, *33*, 14339.
(48) Roberts, L. M.; Lindahl, P. A. *J. Am. Chem. Soc.* **1995**, *117*, 2565.
(49) Guigliarelli, D.; More, C.; Fournel, A.; Asso, M.; Hatchikian, E. C.; Williams, R.; Cammack, R.; Bertrand, P. *Biochemistry* **1995**, *34*, 4781.
(50) (a) van der Zwaan, J. W.; Albracht, S. P. J.; Fontijn, R. D.; Slater, E. C. *FEBS Lett.* **1985**, *179*, 271. (b) Whitehead, J. P.; Gurbiel, R. J.; Bagyinka, C.; Hoffman, B. M.; Maroney, M. J. *J. Am. Chem. Soc.* **1993**, *115*, 5629.

flexibility for the stabilization of various metal oxidation states.[51] In the hydrogenase context, future ligand design must address these issues as well as the inclusion of a binuclear metal site, and stable aqueous systems must be sought where anion effects may be absent and H/D isotope exchange can be examined. As it stands, however, the $[Ni(psnet)]^+$ system serves as the most thoroughly scrutinized system for Ni-mediated formation of $H_2$. Whether nickel alone, or in necessary concert with iron, is the site of hydrogen activation is unknown and will be difficult to determine.

**Acknowledgment.** This research was supported by NSF Grants CHE 92-08387 and 94-23830. We thank Professor W. H. Armstrong for use of a magnetic susceptibility balance, and Drs. J. D. Franolic, J. R. Long, M. J. Scott, and A. Tyler for experimental assistance.

## Appendix

**Determination of $[Cl^-]$.** Equations to determine the actual chloride concentration after homoconjugation equilibrium 9 is considered are presented below. Equations 1A and 2A apply to experiments in which HCl and $Bu_4NCl$ are present, while eq 3A applies to experiments in which HCl is the only chloride source.

When $[Cl^-]_0 > [HCl]_0$:

$$[Cl^-] = ([Cl^-]_0 - [HCl]_0) + \{[(K_f[Cl^-]_0 - K_f[HCl]_0 + 1)^2 + 4K_f[HCl]_0]^{1/2} - (K_f[Cl^-]_0 - K_f[HCl]_0 + 1)/2K_f\} \quad (1A)$$

When $[HCl]_0 > [Cl^-]_0$:

$$[Cl^-] = \{[(K_f[HCl]_0 - K_f[Cl^-]_0 + 1)^2 + 4K_f[Cl^-]_0]^{1/2} - (K_f[HCl]_0 - K_f[Cl^-]_0 + 1)/2K_f\} \quad (2A)$$

When $[Cl^-]_0 = 0$:

$$[Cl^-] = \left[\frac{K_a[HCl]_0}{1 + K_f[HCl]_0}\right]^{1/2} \quad (3A)$$

**Kinetics Analysis of Scheme 1.** Equation 4A employs the simplifying assumption $k_6 = k_7 = k_8$. Substitution for the ion-pairing equilibria in eq 11 in terms of $[Ni{-}H^{2+}]$ yields eq 5A.

$$-d[Ni^I]/dt = k_6([Ni{-}HCl^+] + [Ni{-}HCl|Cl^-])^2 + k_9[Ni{-}H^{2+}|2Cl^-] \quad (4A)$$

$$\frac{-d[Ni^I]}{dt} = k_6\frac{(K_2K_4 + K_2K_3K_5[Cl^-])^2[Ni{-}H^{2+}]^2[Cl^-]^2}{(1 + K_2[Cl^-] + K_2K_3[Cl^-]^2)^2} + \frac{k_9K_2K_3[Cl^-]^2[Ni{-}H^{2+}]}{(1 + K_2[Cl^-] + K_2K_3[Cl^-]^2)} \quad (5A)$$

Substitution for $[Ni{-}H^{2+}]$ in terms of [HCl] and $[Ni^I]$ using eqs 7 and 10, respectively, affords eq 6A. The conservation eq 7A and eq 9 are used to express [HCl] in terms of the initial HCl concentration, $[HCl]_0$, in eq 8A. Substitution for [HCl]

$$\frac{-d[Ni^I]}{dt} = k_6K_a^2K_1^2\frac{(K_2K_4 + K_a^{1/2}K_2K_3K_5[HCl]^{1/2})^2[Ni^I]^2[HCl]^2}{(1 + K_2[Cl^-] + K_2K_3[Cl^-]^2)^2} + \frac{k_9K_aK_1K_2K_3[Cl^-][Ni^I][HCl]}{(1 + K_2[Cl^-] + K_2K_3[Cl^-]^2)} \quad (6A)$$

$$[HCl]_0 = [HCl] + [HCl_2^-] = [HCl](1 + K_f[Cl^-]) \quad (7A)$$

$$[HCl] = [HCl]_0/(1 + K_f[Cl^-]) \quad (8A)$$

into eq 6A, using eq 8A, yields eq 9A. Equation 9A represents the general form of the rate law. At the low chloride concentrations that prevail when HCl is the sole chloride source, $K_f[Cl^-] \ll 1$ and $K_2[Cl^-] + K_2K_3[Cl^-] \ll 1$ (from the data fitted in Figure 11). Therefore, eq 9A simplifies to eq 12.

$$\frac{-d[Ni^I]}{dt} = k_6K_a^2K_1^2\{(K_2K_4 + K_a^{1/2}K_2K_3K_5[[HCl]_0/(1 + K_f[Cl^-])]^{1/2})^2[Ni^I]^2([HCl]_0/(1 + K_f[Cl^-]))^2/(1 + K_2[Cl^-] + K_2K_3[Cl^-]^2)^2\} + \frac{k_9K_aK_1K_2K_3[Cl^-][Ni^I][HCl]_0}{(1 + K_2[Cl^-] + K_2K_3[Cl^-]^2)(1 + K_f[Cl^-])} \quad (9A)$$

**Kinetics Analysis of Scheme 2.** Equation 10A employs the simplifying assumption $k_6 = k_7 = k_8 = k_{14} = k_{15} = k_{16}$.

$$-d[Ni^I]/dt = k_6([Ni{-}HCl^+] + [Ni{-}HCl^+|Cl^-] + [Ni{-}HCl^+|PF_6^-])^2 \quad (10A)$$

Substitution for the ion-pairing equilibria in eqs 11 and 15 in terms of $[Ni{-}H^{2+}]$ yields eq 11A. Substitution for $[Ni{-}H^{2+}]$ in terms of $[Ni^I]$ and $[HCl]_0$ using eqs 7, 10, and 8A yields eq 12A. Using the assumptions outlined in the last step of the derivation for Scheme 1, one sees that eq 12A simplifies to eq 19.

$$-d[Ni^I]/dt = k_6[Ni{-}H^{2+}]^2[Cl^-]^2((K_2K_4 + K_2K_3K_5[Cl^-] + K_{10}K_{12}K_{13}[PF_6^-])/(1 + K_2[Cl^-] + K_2K_3[Cl^-]^2 + K_{10}[PF_6^-] + K_{10}K_{11}[PF_6^-]^2 + K_{10}K_{12}[PF_6^-][Cl^-]))^2 \quad (11A)$$

$$-d[Ni^I]/dt = [k_6K_a^2K_1^2[Ni^I]^2[HCl]_0^2/(1 + K_f[Cl^-])^2]((K_2K_4 + K_2K_3K_5[Cl^-] + K_{10}K_{12}K_{13}[PF_6^-])/(1 + K_2[Cl^-] + K_2K_3[Cl^-]^2 + K_{10}[PF_6^-] + K_{10}K_{11}[PF_6^-]^2 + K_{10}K_{12}[PF_6^-][Cl^-]))^2 \quad (12A)$$

**Kinetics Analysis of Scheme 3.**

$$-d[Ni^I]/dt = k_{17}[Ni{-}H^{2+}]^2 \quad (13A)$$

Substitution for $[Ni{-}H^{2+}]$ in terms of $[Ni^I]$ and $[H^+]$ using eq 10 yields eq 14A. The conservation eq 15A and eqs 7−9 lead to eq 16A. Substitution for $[H^+]$ in eq 14A leads to the final form of the rate law described in eq 24.

(51) Note that undesired bimolecular reactions, such as those which form $Fe^{III}OFe^{III}$ and $O{=}Mo^{V}OMo^{V}{=}O$ bridges instead of the desired $FeO_2$[52a] and $Mo^{IV}O/Mo^{VI}O_2$[52bc] units, respectively, have been overcome by the use of sterically encumbered ligands.

(52) (a) Momenteau, M.; Reed, C. A. *Chem. Rev.* **1994**, *94*, 659. (b) Holm, R. H. *Coord. Chem. Rev.* **1990**, *100*, 183. (c) Schultz, B. E.; Gheller, S. F.; Muetterties, M. C.; Scott, M. J.; Holm, R. H. *J. Am. Chem. Soc.* **1993**, *115*, 2714.

$$-\mathrm{d}[\mathrm{Ni^I}]/\mathrm{d}t = k_{17}K_1[\mathrm{Ni^I}]^2[\mathrm{H^+}]^2 \quad (14A)$$

$$[\mathrm{H^+}] = [\mathrm{Cl^-}] + [\mathrm{HCl_2^-}] \quad (15A)$$

$$[\mathrm{H^+}] = (K_a[\mathrm{HCl}]_0 + K_aK_f[\mathrm{HCl}]_0^2)^{1/2} \quad (16A)$$

**Kinetics Analysis of Scheme 4.**

$$-\mathrm{d}[\mathrm{Ni^I}]/\mathrm{d}t = k_{18}[\mathrm{Ni^I}][\mathrm{Ni{-}H^{2+}}] \quad (17A)$$

Substitution for $[\mathrm{Ni{-}H^{2+}}]$ in eq 17A using eq 10 yields eq 18A. Substitution for $[\mathrm{H^+}]$ in eq 18A using eq 16A leads to the final form of the rate law presented in eq 25.

$$-\mathrm{d}[\mathrm{Ni^I}]/\mathrm{d}t = k_{18}K_1[\mathrm{Ni^I}]^2[\mathrm{H^+}] \quad (18A)$$

**Supporting Information Available:** Tables of crystallographic data for the compounds in Table 1, including crystal data and intensity collection parameters, and of positional and thermal parameters and interatomic distances and angles (11 pages). Ordering information is given on any current masthead page.

IC960216V